

Kernel Method for Detecting Higher Order Interactions in multi-view Data: An Application to Imaging, Genetics, and Epigenetics

Md. Ashad Alam¹, Hui-Yi Lin², Vince Calhoun³ and Yu-Ping Wang¹

¹Department of Biomedical Engineering, Tulane University
New Orleans, LA 70118, USA

² Biostatistics Program, Louisiana State University Health Sciences Center
New Orleans, LA 70112, USA

³Department of Electrical and Computer Engineering, The University of New Mexico
Albuquerque, NM 87131, USA

Abstract

Technological advances are enabling us to collect multiple types of data at an increasing depth and resolution while decreasing the labor needed to compile and analyze it. A central goal of multimodal data integration is to understand the interaction effects of different features. Understanding the complex interaction among multimodal datasets, however, is challenging. In this study, we tested the interaction effect of multimodal datasets using a novel method called the kernel method for detecting higher order interactions among biologically relevant multi-view data. Using a semiparametric method on a reproducing kernel Hilbert space (RKHS), we used a standard mixed-effects linear model and derived a score-based variance component statistic that tests for higher order interactions between multi-view data. The proposed method offers an intangible framework for the identification of higher order interaction effects (e.g., three way interaction) between genetics, brain imaging, and epigenetic data. Extensive numerical simulation studies were first conducted to evaluate the performance of this method. Finally, this method was evaluated using data from the Mind Clinical Imaging Consortium (MCIC) including single nucleotide polymorphism (SNP) data, functional magnetic resonance imaging (fMRI) scans, and deoxyribonucleic acid (DNA) methylation data, respectively, in schizophrenia patients and healthy controls. We treated each gene-derived SNPs, region of interest (ROI) and gene-derived DNA methylation as a single testing unit, which are combined into triplets for evaluation. In addition, cardiovascular disease risk factors such as age, gender, and body mass

index were assessed as covariates on hippocampal volume and compared between triplets. Our method identified 13-triplets (p -values ≤ 0.001) that included 6 gene-derived SNPs, 10 ROIs, and 6 gene-derived DNA methylations that correlated with changes in hippocampal volume, suggesting that these triplets may be important in explaining schizophrenia-related neurodegeneration. With strong evidence (p -values ≤ 0.000001), the triplet (**MAGI2**, **CRBLCrus1.L**, **FBXO28**) has the potential to distinguish schizophrenia patients from the healthy control variations. This novel method may shed light on other disease processes in the same manner, which may benefit from this type of multimodal analysis.

keywords: Multimodal data, Higher order interaction, Kernel methods, Imaging genetics, Imaging epigenetics, and Schizophrenia.

1 Introduction

The advancements in data science technology over the last decade has rapidly evolved to collect multi-view data, which has emerged to provide a comprehensive way to explore statistical structures and information embedded in the relationship between datasets. The integration of imaging and genetic information into a format capable of predicting disease phenotypes, however, continues to be challenging problem.

One of the goals of imaging genetics is the modeling and understanding of how genetic variations influence the structure and function of brain disease. This goal can be achieved by collating multimodal data including functional magnetic resonance imaging (fMRI), structural MRI (sMRI), and positron emission tomography (PET) scans with single nucleotide polymorphisms (SNPs), deoxyribonucleic acid (DNA) methylations, gene expression (GE), transcriptomics, epigenomics, and proteomics factors. Numerous studies have suggested that these different factors do not act in isolation, but rather they interact at multiple levels and depend on one another in an intertwined manner (Calhoun & Sui, 2016; Pearlson, Liu, & Calhoun, 2015). Extracting the interaction effects from within and among data sets, however, remains a challenge for multi-view data analysis (J. Li et al., 2015; Chekouo, Stingo, Guindani, & Do, 2016; Zheng, Cai, Ding, Nie, & Hung, 2015; Zhao, Qiao, F. Shi, & Shen, 2016; M. Liu, Min, Y. Gao, & Shen, 2016). Figure 1 illustrates how the interaction effects of different data sets can be used to model and predict human illness.

To date, both genetic techniques and brain imaging have played a substantial role in detecting disease phenotypes. For example, by correlating imaging and genetic data, it has been shown that certain genes affect specific brain functions, connectivity, and serve as risk predictors for certain diseases. (Jahanshad et al., 2012; Lin, Callhoun, & Wang, 2014; Bis, DeCarli, & et al., 2012; Ja-

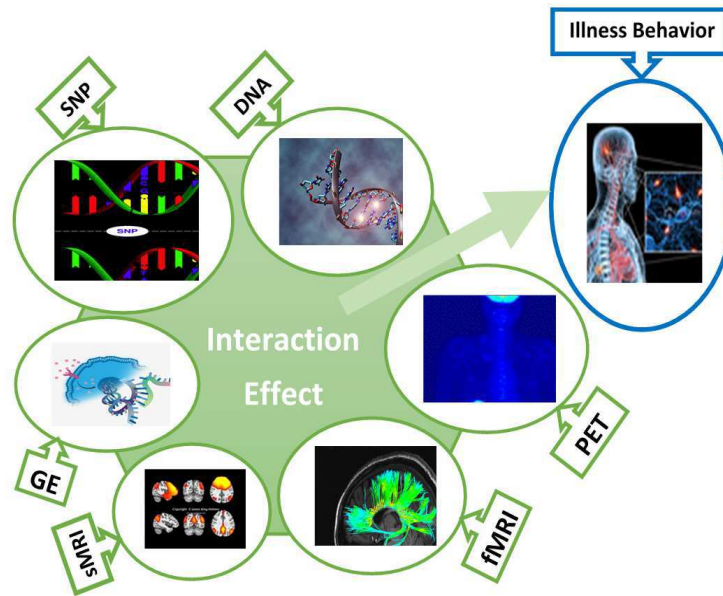


Figure 1: An illustration of the different imaging genetics and epigenetics data along with their interaction effect on human behavior. Note, SNP: single nucleotide polymorphism, DNA: deoxyribonucleic acid methylations, PET: positron emission tomography (PET), fMRI: functional magnetic resonance imaging (fMRI), sMRI: structural MRI, GE: gene expression.

hanshad & X. Hua, 2013). Additionally, (Bis et al., 2012) have identified genetic variants affecting the volume of the hippocampus, which could be used as predictors of cognitive decline and dementia (Jahanshad & X. Hua, 2013). As shown in (Wen et al., 2017), accurate identification of Tourette’s syndrome in children has notably improved using multi-view features as compared to relying solely on one view. Accumulating evidence also shows that the inherent genetic variations for complex traits can sometimes be explained by the joint analysis of multiple genetic features with environmental factors.

Schizophrenia (SZ) is a complex brain disorder that affects how a person thinks, feels and acts, which is thought to be caused through an interplay of genetic effects, brain region, and DNA methylation abnormalities (Richfield, Alam, Calhoun, & Wang, 2017). Studies using neurological tests and brain imaging technologies (fMRI and PET) have been used to examine functional differences in brain activity that seem to arise within the frontal lobes, hippocampus and temporal lobes (Van & Kapur, 2009; Kircher & Renate, 2005). Many researchers have shown that genetic alterations at the mRNA and SNP level, however, also play a significant role in SZ (Chang, Kruger, Kustra, & Zhang, 2013; Lencz et al., 2007). Thus, only focusing on brain imaging data is not sufficient in the identification of the related risk factors for SZ (Potkin, T. G. M. Van, Ling, Macciardi, & Xie, 2015). To address this, (Chekouo et al., 2016) have developed the ROI-SNP network for the selection of

discriminatory markers using brain imaging and genetics information.

A number of studies suggest that epigenetics also has a role in SZ disease susceptibility. Genome-wide DNA methylation analysis of human brain tissue from SZ patients shows a heritable epigenetic modification, which can regulate gene expression. The cell specific differences in chromatin structure that influence cell development, including DNA methylation, have emerged as a potential explanation for the non-Mendelian inheritance of SZ (Wockner et al., 2014). There is also evidence on epigenetic alterations in the blood and central nervous system of patients with SZ, and it has been shown that methylation status in brain tissue from SZ patients varies significantly from controls (Aberg, McClay, Nerella, & et al., 2014; Montano, Tauband, Jaffe, Briem, & et al., 2016). In this paper, we consider the interaction effects among the genetics, brain imaging, and epigenetics data on hippocampal volume measurements between SZ patients and healthy controls using a novel kernel method for detecting these higher order interactions.

Many advancements in multimodal fusion methods have utilized such approaches as co-training, multi-view learning, subspace learning, multi-view embedding, and kernel multiple learning, to analyze multi-view data of biological relevance (Xu, Tao, & Xu, 2013). However, due to the large number of genes, SNPs, DNA methylations and different types of imaging, positive definite kernel based methods have become a popular and effective tool for conducting genome-wide association studies (GWASs) and imaging genetics, especially for identifying genes associated with diseases (S. Li & Cui, 2012; Ge et al., 2015; Alam, Calhoun, & Wang, 2016; Alam, Komori, Calhoun, & Wang, 2016). Kernel methods are emerging as innovative techniques that map data from high dimension input spaces to a kernel feature space using a nonlinear function. The main advantage of these methods is to combine statistics and geometry in an effective way (Hofmann, Schölkopf, & Smola, 2008). Kernel methods offer useful algorithms to learn how a large number of genetic variants are associated with complex phenotypes, to help explore the relationship between the genetic markers and the outcome of interest (Camps-Valls, Rojo-Alvarez, & Martinez-Romon, 2007; S. Yu & Moreau, 2011; Alam, 2014; Alam & Fukumizu, 2015; Schölkopf, Smola, & Müller, 1998; Kung, 2014).

In genetics, the detection of gene-gene interactions or co-associations in most methods are divided into two types: SNP based and gene-based methods in GWASs. In the last decade, a number of statistical methods have been used to detect gene-gene interactions (GGIs). Logistic regression, multifactor dimensionality reduction, linkage disequilibrium and entropy based statistics are examples of such methods (Hieke, Binder, Nieters, & Schumacher, 2014; Wan et al., 2010). While most of these methods are based on the unit association of the SNPs, testing the associations between

the phenotype and SNPs has limitations and is not sufficient for interpretation of GGIs (Yuan et al., 2012). In GWASs, gene-based methods are always more effective than the ones based only on a SNP, and powerful tools for multivariate gene-based genome-wide associations have been proposed (Sluis et al., 2015).

In recent years, linear, kernel, and robust canonical correlation based U statistic have been utilized to identify gene-gene co-associations (Peng, Zhao, & Xue, 2010; Alam, Komori, et al., 2016). (S. Li & Cui, 2012) have proposed a model-based kernel machine method for GGIs. In addition, (Ge et al., 2015) have also proposed a kernel machine method for detecting effects of interactions between multi-variable sets. This is an extended model of (S. Li & Cui, 2012) to jointly model the genetics and non-genetic features, and their interactions. While these methods could ultimately shed light on novel features of the etiology of complex diseases, they cannot be reliably used in multi-view data sets. Thus, there exists a need to extend kernel machine based methods.

The contribution of this paper, therefore, is threefold. By examining the three-way interaction effects between triplet data sets combining genetics, imaging, and epigenetics, we hope to shed light on the phenotype features associated with disease mechanisms. This is done iteratively. First, we propose a novel semiparametric method on a reproducing kernel Hilbert space (RKHS) to study the interaction effects among the multiple-view datasets. We name a kernel method for detecting higher order interactions (KMDHOI) and include the pairwise and higher order Hadamard product of the features from different views. Second, we formulate the problem as a standard mixed-effect linear model to derive a score-based variance component test for the higher order interactions. The proposed method offers a flexible framework to account for the main (single), pairwise, triplet, other higher order effects and test for the overall higher order effects. Finally, we validate the proposed method on both simulation and the Mind Clinical Imaging Consortium (MCIC) data (J. Chen et al., 2012; Gollub et al., 2013).

The remainder of this paper is organized as follows. In Section 2, we propose a standard mixed-effects linear model to derive score-based variance component test for higher order interaction. In Section 3, we propose statistical testing for higher order interaction effects. The relevant methods are discussed in Section 4. In Section 5, we describe the experiments conducted on both synthesized and the imaging genetics data sets. We conclude the paper with a discussion of major findings and future research in Section 6. Details of the theoretical analysis for the proposed method, Satterthwaite approximation to the score test, and supplementary tables and figures on application to imaging genetics and epigenetics can be found in the appendix.

2 Method

In kernel methods, the nonlinear feature map is given by a **positive definite kernel**, which provides nonlinear methods for data analysis. It is known (Aronszajn, 1950) that a positive definite kernel k is associated with a Hilbert space \mathcal{H} , called **reproducing kernel Hilbert space** (RKHS), consisting of functions on \mathcal{X} so that the function value is reproduced by the kernel; namely, for any function $f \in \mathcal{H}$ and a point $X \in \mathcal{X}$, the function value $f(X)$ is $f(X) = \langle f(\cdot), k(\cdot, X) \rangle_{\mathcal{H}}$, where $\langle \cdot, \cdot \rangle_{\mathcal{H}}$ in the inner product of \mathcal{H} is called the reproducing property. Replacing f with $k(\cdot, \tilde{X})$ yields $k(X, \tilde{X}) = \langle k(\cdot, X), k(\cdot, \tilde{X}) \rangle_{\mathcal{H}}$ for any $X, \tilde{X} \in \mathcal{X}$. A symmetric kernel $k(\cdot, \cdot)$ defined on a space \mathcal{X} is called **positive definite**, if for an arbitrary number of points $X_1, \dots, X_n \in \mathcal{X}$ the Gram matrix $(k(X_i, Y_j))_{ij}$ is positive semi-definite. To transform data for extracting nonlinear features, the mapping $\Phi : \mathcal{X} \rightarrow \mathcal{H}$ is defined as $\Phi(X) = k(\cdot, X)$, which is a function of the first argument. This map is called the **feature map**, and the vector $\Phi(X)$ in \mathcal{H} is called the **feature vector**. The inner product of two feature vectors is then $\langle \Phi(X), \Phi(\tilde{X}) \rangle_{\mathcal{H}} = k(X, \tilde{X})$. This is known as the **kernel trick**. By this trick the kernel can evaluate the inner product of any two feature vectors efficiently without knowing an explicit form of $\Phi(\cdot)$.

2.1 Model setting

Assuming that we have n independent identical distributed (IID) subjects y_i ($i = 1, 2, \dots, n$) with $(q - 1)$ covariates $X_i = [X_{i1}, X_{i2} \dots X_{i(q-1)}]^T$ and m -view datasets, $\mathbf{M}_i^{(1)}, \dots, \mathbf{M}_i^{(m)}$. In the following semiparametric model, we associate the output y_i with covariates including intercept and m -view datasets:

$$y_i = X_i^T \boldsymbol{\beta} + f(\mathbf{M}_i^{(1)}, \dots, \mathbf{M}_i^{(m)}) + \epsilon_i, \quad (1)$$

where X_i is a $q \times 1$ vector of covariates including intercept for the i -th subject, $\boldsymbol{\beta}$ is a $q \times 1$ vector of fixed effects, f is an unknown function on the product domain, $\mathcal{M} = \mathcal{M}^{(1)} \otimes \mathcal{M}^{(2)} \otimes \dots \otimes \mathcal{M}^{(m)}$ with $\mathbf{M}_i^{(\ell)} \in \mathcal{M}_\ell$, $\ell = 1, 2, \dots, m$ and the error ϵ_i 's are IID as normal with mean zero and variance σ^2 ,

$\epsilon_i \sim \text{NIID}(0, \sigma^2)$). According to the ANOVA decomposition, the function, f can be extended as:

$$f(\mathbf{M}_i^{(1)}, \dots, \mathbf{M}_i^{(m)}) = \sum_{\ell=1}^m h_{\mathbf{M}^{(\ell)}}(\mathbf{M}_i^{(\ell)}) + \sum_{\ell_1 > \ell_2} h_{\mathbf{M}^{(\ell_1), \mathbf{M}^{(\ell_2)}}}(\mathbf{M}_i^{(\ell_1)}, \mathbf{M}_i^{(\ell_2)}) + \sum_{\ell_1 > \ell_2 > \ell_3} h_{\mathbf{M}^{(\ell_1) \times \mathbf{M}^{(\ell_2)} \times \mathbf{M}^{(\ell_3)}}}(\mathbf{M}_i^{(\ell_1)}, \mathbf{M}_i^{(\ell_2)}, \mathbf{M}_i^{(\ell_3)}) + \dots + h_{\mathbf{M}^{(1) \times \mathbf{M}^{(2)} \times \mathbf{M}^{(3)} \times \dots \times \mathbf{M}^{(m)}}}(\mathbf{M}_i^{(1)}, \mathbf{M}_i^{(2)}, \dots, \mathbf{M}_i^{(m)}), \quad (2)$$

where $h_{\mathbf{M}^{(\ell)}}(\mathbf{M}_i^{(\ell)})$'s ($\ell : 1, 2, \dots, m$) are the main effects for the respective dataset, $h_{\mathbf{M}^{(\ell_1), \mathbf{M}^{(\ell_2)}}}(\mathbf{M}_i^{(\ell_1)}, \mathbf{M}_i^{(\ell_2)})$ are pairwise interactions effects, $h_{\mathbf{M}^{(\ell_1) \times \mathbf{M}^{(\ell_2)}, \mathbf{M}^{(\ell_3)}}}(\mathbf{M}_i^{(\ell_1)}, \mathbf{M}_i^{(\ell_2)}, \mathbf{M}_i^{(\ell_3)})$ are the interactions effects of the three dataset and so on. The functional space, RKHS, is decomposes as:

$$\mathcal{H} = \mathcal{H}_{\mathbf{M}^{(1)}} \oplus \mathcal{H}_{\mathbf{M}^{(2)}} \oplus \dots \oplus \mathcal{H}_{\mathbf{M}^{(m)}} \oplus \mathcal{H}_{\mathbf{M}^{(1) \times \mathbf{M}^{(2)}}} \oplus \mathcal{H}_{\mathbf{M}^{(1) \times \mathbf{M}^{(3)}}} \oplus \dots \oplus \mathcal{H}_{\mathbf{M}^{(1) \times \mathbf{M}^{(m)}}} \oplus \mathcal{H}_{\mathbf{M}^{(2) \times \mathbf{M}^{(3)}}} \oplus \dots \oplus \mathcal{H}_{\mathbf{M}^{(1) \times \mathbf{M}^{(2)} \times \mathbf{M}^{(3)}}} \oplus \dots \oplus \mathcal{H}_{\mathbf{M}^{(1) \times \mathbf{M}^{(2)} \times \dots \times \mathbf{M}^{(m)}}}, \quad (3)$$

equipped with an inner product, $\langle \cdot, \cdot \rangle$ and a norm $\| \cdot \|_{\mathcal{H}}$. If $m = 1$, Eq. (1) becomes simple semiparametric regression model as shown in (D. Liu, Lin, & Ghosh, 2007). (S. Li & Cui, 2012) and (Ge et al., 2015) have proposed similar models (special case of Eq. (1), $m = 2$) for detecting interaction effects among multidimensional variable sets.

Specifically, in our case we have three data sets. To do this, we assume that we have n IID subjects under investigation; y_i ($i = 1, 2, \dots, n$) is a quantitative phenotype for the i -th subject (say, hippocampal volume derived from structural MRI scan). We associate the clinical covariates (e.g., age, weight, height) with three views: genetics, imaging, and epigenetics (gene-derived SNP, ROIs, and gene-derived DNA methylation). Let \mathbf{X}_i denote the $(q-1)$ covariates, where X_{ij} , $j = 1, 2, \dots, (q-1)$ is a measure of the i -th subject. Let $M_i^{(1)} = [M_{i1}^{(1)}, M_{i2}^{(1)}, \dots, M_{is}^{(1)}]$, $M_i^{(2)} = [M_{i1}^{(2)}, M_{i2}^{(2)}, \dots, M_{is}^{(2)}]$ and $M_i^{(3)} = [M_{i1}^{(3)}, M_{i2}^{(3)}, \dots, M_{is}^{(3)}]$ be a genes-derived SNP with s SNP markers, a ROI with r voxels of the fMRI scan, and a gene-derived DNA methylation with d methylation profiles of the i -th subject, respectively. Under this setting, Eq. (1), Eq. (2) and Eq. (3) become:

$$y_i = X_i^T \boldsymbol{\beta} + f(\mathbf{M}_i^{(1)}, \mathbf{M}_i^{(2)}, \mathbf{M}_i^{(3)}) + \epsilon_i, \quad (4)$$

$$f(\mathbf{M}_i^{(1)}, \mathbf{M}_i^{(2)}, \mathbf{M}_i^{(3)}) = h_{\mathbf{M}^{(1)}}(\mathbf{M}_i^{(1)}) + h_{\mathbf{M}^{(2)}}(\mathbf{M}_i^{(2)}) + h_{\mathbf{M}^{(3)}}(\mathbf{M}_i^{(3)}) + h_{\mathbf{M}^{(1) \times \mathbf{M}^{(2)}}}(\mathbf{M}_i^{(1)}, \mathbf{M}_i^{(2)}) + h_{\mathbf{M}^{(1) \times \mathbf{M}^{(3)}}}(\mathbf{M}_i^{(1)}, \mathbf{M}_i^{(3)}) + h_{\mathbf{M}^{(2) \times \mathbf{M}^{(3)}}}(\mathbf{M}_i^{(2)}, \mathbf{M}_i^{(3)}) + h_{\mathbf{M}^{(1) \times \mathbf{M}^{(2)} \times \mathbf{M}^{(3)}}}(\mathbf{M}_i^{(1)}, \mathbf{M}_i^{(2)}, \mathbf{M}_i^{(3)}), \quad (5)$$

and

$$\mathcal{H} = \mathcal{H}_{\mathbf{M}^{(1)}} \oplus \mathcal{H}_{\mathbf{M}^{(2)}} \oplus \mathcal{H}_{\mathbf{M}^{(3)}} \oplus \mathcal{H}_{\mathbf{M}^{(1)} \times \mathbf{M}^{(2)}} \oplus \mathcal{H}_{\mathbf{M}^{(1)} \times \mathbf{M}^{(3)}} \oplus \mathcal{H}_{\mathbf{M}^{(2)} \times \mathbf{M}^{(3)}} \oplus \mathcal{H}_{\mathbf{M}^{(1)} \times \mathbf{M}^{(2)} \times \mathbf{M}^{(3)}}, \quad (6)$$

respectively. Here $\mathcal{H}_{\mathbf{M}^{(1)}}$, $\mathcal{H}_{\mathbf{M}^{(2)}}$ and $\mathcal{H}_{\mathbf{M}^{(3)}}$, and $\mathcal{H}_{\mathbf{M}^{(1)} \times \mathbf{M}^{(2)}}$, $\mathcal{H}_{\mathbf{M}^{(1)} \times \mathbf{M}^{(3)}}$ and $\mathcal{H}_{\mathbf{M}^{(2)} \times \mathbf{M}^{(3)}}$, and $\mathcal{H}_{\mathbf{M}^{(1)} \times \mathbf{M}^{(2)} \times \mathbf{M}^{(3)}}$ are RKHSs functions on \mathcal{M}_1 , \mathcal{M}_2 and \mathcal{M}_3 , and $\mathcal{M}_1 \times \mathcal{M}_2$, $\mathcal{M}_1 \times \mathcal{M}_3$ and $\mathcal{M}_2 \times \mathcal{M}_3$ and $\mathcal{M}_1, \mathcal{M}_2 \times \mathcal{M}_3$, respectively. The notation \oplus is a direct sum of RKHS.

2.2 Model estimation

We can estimate the function $f \in \mathcal{H}$ by minimizing the penalized squared error loss function of Eq. (4) as:

$$\mathcal{L}(\mathbf{y}, \boldsymbol{\beta}, f) = \frac{1}{2} \sum_{i=1}^n [y_i - X_i^T \boldsymbol{\beta} - f(\mathbf{M}_i^{(1)}, \mathbf{M}_i^{(2)}, \mathbf{M}_i^{(3)})]^2 + \frac{\lambda}{2} \mathcal{J}(f) \quad (7)$$

where $\mathcal{J}(\cdot) = \|\cdot\|_{\mathcal{H}}^2$ is a roughness penalty with tuning parameter λ . It is known that the complete function space of Eq. (6), \mathcal{H} , has the orthogonal decomposition. Hence the function $\mathcal{J}(\cdot)$ can be decomposed accordingly. Eq. (7) then becomes:

$$\begin{aligned} \mathcal{L}(\mathbf{y}, \boldsymbol{\beta}, f) &= \frac{1}{2} \sum_{i=1}^n [y_i - X_i^T \boldsymbol{\beta} - h_{\mathbf{M}^{(1)}}(\mathbf{M}_i^{(1)}) - h_{\mathbf{M}^{(2)}}(\mathbf{M}_i^{(2)}) - h_{\mathbf{M}^{(3)}}(\mathbf{M}_i^{(3)}) - h_{\mathbf{M}^{(1)} \times \mathbf{M}^{(2)}}(\mathbf{M}_i^{(1)}, \mathbf{M}_i^{(2)}) \\ &\quad - h_{\mathbf{M}^{(1)} \times \mathbf{M}^{(3)}}(\mathbf{M}_i^{(1)}, \mathbf{M}_i^{(3)}) - h_{\mathbf{M}^{(2)} \times \mathbf{M}^{(3)}}(\mathbf{M}_i^{(2)}, \mathbf{M}_i^{(3)}) - h_{\mathbf{M}^{(1)} \times \mathbf{M}^{(2)} \times \mathbf{M}^{(3)}}(\mathbf{M}_i^{(1)}, \mathbf{M}_i^{(2)}, \mathbf{M}_i^{(3)})]^2 \\ &\quad + \frac{\lambda^{(1)}}{2} \|h_{\mathbf{M}^{(1)}}\|^2 + \frac{\lambda^{(2)}}{2} \|h_{\mathbf{M}^{(2)}}\|^2 + \frac{\lambda^{(3)}}{2} \|h_{\mathbf{M}^{(3)}}\|^2 + \frac{\lambda^{(1 \times 2)}}{2} \|h_{\mathbf{M}^{(1)} \times \mathbf{M}^{(2)}}\|^2 + \frac{\lambda^{(1 \times 3)}}{2} \|h_{\mathbf{M}^{(1)} \times \mathbf{M}^{(3)}}\|^2 \\ &\quad + \frac{\lambda^{(2 \times 3)}}{2} \|h_{\mathbf{M}^{(2)} \times \mathbf{M}^{(3)}}\|^2 + \frac{\lambda^{(1 \times 2 \times 3)}}{2} \|h_{\mathbf{M}^{(1)} \times \mathbf{M}^{(2)} \times \mathbf{M}^{(3)}}\|^2 \quad (8) \\ &= [\mathbf{y} - \mathbf{X}\boldsymbol{\beta} - \mathbf{h}_{\mathbf{M}^{(1)}} - \mathbf{h}_{\mathbf{M}^{(2)}} - \mathbf{h}_{\mathbf{M}^{(3)}} - \mathbf{h}_{\mathbf{M}^{(1)} \times \mathbf{M}^{(2)}} - \mathbf{h}_{\mathbf{M}^{(1)} \times \mathbf{M}^{(3)}} \\ &\quad - \mathbf{h}_{\mathbf{M}^{(2)} \times \mathbf{M}^{(3)}} - \mathbf{h}_{\mathbf{M}^{(1)} \times \mathbf{M}^{(2)} \times \mathbf{M}^{(3)}}]^2 + \frac{\lambda^{(1)}}{2} \|h_{\mathbf{M}^{(1)}}\|^2 + \frac{\lambda^{(2)}}{2} \|h_{\mathbf{M}^{(2)}}\|^2 + \frac{\lambda^{(3)}}{2} \|h_{\mathbf{M}^{(3)}}\|^2 \\ &\quad + \frac{\lambda^{(1 \times 2)}}{2} \|h_{\mathbf{M}^{(1)} \times \mathbf{M}^{(2)}}\|^2 + \frac{\lambda^{(1 \times 3)}}{2} \|h_{\mathbf{M}^{(1)} \times \mathbf{M}^{(3)}}\|^2 + \frac{\lambda^{(2 \times 3)}}{2} \|h_{\mathbf{M}^{(2)} \times \mathbf{M}^{(3)}}\|^2 + \frac{\lambda^{(1 \times 2 \times 3)}}{2} \|h_{\mathbf{M}^{(1)} \times \mathbf{M}^{(2)} \times \mathbf{M}^{(3)}}\|^2, \end{aligned}$$

where $\mathbf{y} = [y_1, y_2, \dots, y_n]^T$, $\mathbf{X} = [X_1, X_2, \dots, X_n]^T$, $\mathbf{h}_{\mathbf{M}^{(1)}} = [h_{\mathbf{M}^{(1)}}(\mathbf{M}_1^{(1)}), h_{\mathbf{M}^{(1)}}(\mathbf{M}_2^{(1)}), \dots, h_{\mathbf{M}^{(1)}}(\mathbf{M}_n^{(1)})]^T$, $\mathbf{h}_{\mathbf{M}^{(2)}} = [h_{\mathbf{M}^{(2)}}(\mathbf{M}_1^{(2)}), h_{\mathbf{M}^{(2)}}(\mathbf{M}_2^{(2)}), \dots, h_{\mathbf{M}^{(2)}}(\mathbf{M}_n^{(2)})]^T$, $\mathbf{h}_{\mathbf{M}^{(3)}} = [h_{\mathbf{M}^{(3)}}(\mathbf{M}_1^{(3)}), h_{\mathbf{M}^{(3)}}(\mathbf{M}_2^{(3)}), \dots, h_{\mathbf{M}^{(3)}}(\mathbf{M}_n^{(3)})]^T$, $\mathbf{h}_{\mathbf{M}^{(1)} \times \mathbf{M}^{(2)}} = [h_{\mathbf{M}^{(1)} \times \mathbf{M}^{(2)}}(\mathbf{M}_1^{(1)}, \mathbf{M}_1^{(2)}), h_{\mathbf{M}^{(1)} \times \mathbf{M}^{(2)}}(\mathbf{M}_2^{(1)}, \mathbf{M}_2^{(2)}), \dots, h_{\mathbf{M}^{(1)} \times \mathbf{M}^{(2)}}(\mathbf{M}_n^{(1)}, \mathbf{M}_n^{(2)})]^T$, $\mathbf{h}_{\mathbf{M}^{(1)} \times \mathbf{M}^{(3)}} = [h_{\mathbf{M}^{(1)} \times \mathbf{M}^{(3)}}(\mathbf{M}_1^{(1)}, \mathbf{M}_1^{(3)}), h_{\mathbf{M}^{(1)} \times \mathbf{M}^{(3)}}(\mathbf{M}_2^{(1)}, \mathbf{M}_2^{(3)}), \dots, h_{\mathbf{M}^{(1)} \times \mathbf{M}^{(3)}}(\mathbf{M}_n^{(1)}, \mathbf{M}_n^{(3)})]^T$, $\mathbf{h}_{\mathbf{M}^{(2)} \times \mathbf{M}^{(3)}} = [h_{\mathbf{M}^{(2)} \times \mathbf{M}^{(3)}}(\mathbf{M}_1^{(2)}, \mathbf{M}_1^{(3)}), h_{\mathbf{M}^{(2)} \times \mathbf{M}^{(3)}}(\mathbf{M}_2^{(2)}, \mathbf{M}_2^{(3)}), \dots, h_{\mathbf{M}^{(2)} \times \mathbf{M}^{(3)}}(\mathbf{M}_n^{(2)}, \mathbf{M}_n^{(3)})]^T$, $\mathbf{h}_{\mathbf{M}^{(1)} \times \mathbf{M}^{(2)} \times \mathbf{M}^{(3)}} = [h_{\mathbf{M}^{(1)} \times \mathbf{M}^{(2)} \times \mathbf{M}^{(3)}}(\mathbf{M}_n^{(1)}, \mathbf{M}_1^{(2)}, \mathbf{M}_1^{(3)}), h_{\mathbf{M}^{(1)} \times \mathbf{M}^{(2)} \times \mathbf{M}^{(3)}}(\mathbf{M}_n^{(1)}, \mathbf{M}_2^{(2)}, \mathbf{M}_2^{(3)}), \dots, h_{\mathbf{M}^{(1)} \times \mathbf{M}^{(2)} \times \mathbf{M}^{(3)}}(\mathbf{M}_n^{(1)}, \mathbf{M}_n^{(2)}, \mathbf{M}_n^{(3)})]^T$,

$\lambda^{(1)}, \lambda^{(2)}, \lambda^{(3)}, \lambda^{(1 \times 2)}, \lambda^{(1 \times 3)}, \lambda^{(2 \times 3)}$ and $\lambda^{(1 \times 2 \times 3)}$ are the positive tuning parameters that trade-off between the model fits and its complexity.

By the representer theorem (Kimeldorf & Wahhba, 1971; Schölkopf & Smola, 2002) and the fact that the reproduction kernel of a product of an RKHS is the product of the reproducing kernels (Aronszajn, 1950), the expanded functions of f in Eq.(8) for arbitrary $\tilde{\mathbf{M}}^{(1)} \in \mathcal{M}^{(1)}$, $\tilde{\mathbf{M}}^{(2)} \in \mathcal{M}^{(2)}$ and $\tilde{\mathbf{M}}^{(3)} \in \mathcal{M}^{(3)}$ can be written as:

$$\begin{aligned}
h_{\mathbf{M}^{(1)}} &= \sum_{i=1}^n \alpha_i^{(1)} k^{(1)}(\tilde{\mathbf{M}}^{(1)}, \mathbf{M}_i^{(1)}), \\
h_{\mathbf{M}^{(2)}} &= \sum_{i=1}^n \alpha_i^{(2)} k^{(2)}(\tilde{\mathbf{M}}^{(2)}, \mathbf{M}_i^{(2)}), \\
h_{\mathbf{M}^{(3)}} &= \sum_{i=1}^n \alpha_i^{(3)} k^{(3)}(\tilde{\mathbf{M}}^{(3)}, \mathbf{M}_i^{(3)}), \\
h_{\mathbf{M}^{(1)} \times \mathbf{M}^{(2)}} &= \sum_{i=1}^n \alpha_i^{(1 \times 2)} k^{(1)}(\tilde{\mathbf{M}}^{(1)}, \mathbf{M}_i^{(1)}) k^{(2)}(\tilde{\mathbf{M}}^{(2)}, \mathbf{M}_i^{(2)}), \\
h_{\mathbf{M}^{(1)} \times \mathbf{M}^{(3)}} &= \sum_{i=1}^n \alpha_i^{(1 \times 3)} k^{(1)}(\tilde{\mathbf{M}}^{(1)}, \mathbf{M}_i^{(1)}) k^{(3)}(\tilde{\mathbf{M}}^{(3)}, \mathbf{M}_i^{(3)}), \\
h_{\mathbf{M}^{(2)} \times \mathbf{M}^{(3)}} &= \sum_{i=1}^n \alpha_i^{(2 \times 3)} k^{(2)}(\tilde{\mathbf{M}}^{(2)}, \mathbf{M}_i^{(2)}) k^{(3)}(\tilde{\mathbf{M}}^{(3)}, \mathbf{M}_i^{(3)}), \\
h_{\mathbf{M}^{(1)} \times \mathbf{M}^{(2)} \times \mathbf{M}^{(3)}} &= \sum_{i=1}^n \alpha_i^{(1 \times 2 \times 3)} k^{(1)}(\tilde{\mathbf{M}}^{(1)}, \mathbf{M}_i^{(1)}) k^{(2)}(\tilde{\mathbf{M}}^{(2)}, \mathbf{M}_i^{(2)}) k^{(3)}(\tilde{\mathbf{M}}^{(3)}, \mathbf{M}_i^{(3)}).
\end{aligned}$$

For each data view, we can define the kernel matrices: $\mathbf{K}^{(1)} = (k^{(1)}(M_i^1, M_j^1))_{ij}$, $\mathbf{K}^{(2)} = (k^{(2)}(M_i^2, M_j^2))_{ij}$, $\mathbf{K}^{(3)} = (k^{(3)}(M_i^3, M_j^3))_{ij}$, $\mathbf{K}^{(1 \times 2)} = \mathbf{K}^{(1)} \odot \mathbf{K}^{(2)}$, $\mathbf{K}^{(1 \times 3)} = \mathbf{K}^{(1)} \odot \mathbf{K}^{(3)}$, $\mathbf{K}^{(2 \times 3)} = \mathbf{K}^{(2)} \odot \mathbf{K}^{(3)}$ and $\mathbf{K}^{(1 \times 2 \times 3)} = \mathbf{K}^{(1)} \odot \mathbf{K}^{(2)} \odot \mathbf{K}^{(3)}$, where \odot is denoted as the element-wise product of two matrices. Now we have

$$\begin{aligned}
\mathbf{h}_{\mathbf{M}^{(1)}} &= \mathbf{K}^{(1)} \boldsymbol{\alpha}^{(1)}, \mathbf{h}_{\mathbf{M}^{(2)}} = \mathbf{K}^{(2)} \boldsymbol{\alpha}^{(2)}, \mathbf{h}_{\mathbf{M}^{(3)}} = \mathbf{K}^{(3)} \boldsymbol{\alpha}^{(3)}, \mathbf{h}_{\mathbf{M}^{(1)} \times \mathbf{M}^{(2)}} = \mathbf{K}^{(1 \times 2)} \boldsymbol{\alpha}^{(1 \times 2)}, \\
\mathbf{h}_{\mathbf{M}^{(1)} \times \mathbf{M}^{(3)}} &= \mathbf{K}^{(1 \times 3)} \boldsymbol{\alpha}^{(1 \times 3)}, \mathbf{h}_{\mathbf{M}^{(2)} \times \mathbf{M}^{(3)}} = \mathbf{K}^{(2 \times 3)} \boldsymbol{\alpha}^{(2 \times 3)}, \mathbf{h}_{\mathbf{M}^{(1)} \times \mathbf{M}^{(2)} \times \mathbf{M}^{(3)}} = \mathbf{K}^{(1 \times 2 \times 3)} \boldsymbol{\alpha}^{(1 \times 2 \times 3)}, \quad (9)
\end{aligned}$$

where $\boldsymbol{\alpha}^{(1)} = [\alpha_1^{(1)}, \alpha_2^{(1)}, \dots, \alpha_n^{(1)}]^T$, $\boldsymbol{\alpha}^{(2)} = [\alpha_1^{(2)}, \alpha_2^{(2)}, \dots, \alpha_n^{(2)}]^T$, $\boldsymbol{\alpha}^{(3)} = [\alpha_1^{(3)}, \alpha_2^{(3)}, \dots, \alpha_n^{(3)}]^T$, $\boldsymbol{\alpha}^{(1 \times 2)} = [\alpha_1^{(1 \times 2)}, \alpha_2^{(1 \times 2)}, \dots, \alpha_n^{(1 \times 2)}]^T$, $\boldsymbol{\alpha}^{(1 \times 3)} = [\alpha_1^{(1 \times 3)}, \alpha_2^{(1 \times 3)}, \dots, \alpha_n^{(1 \times 3)}]^T$, $\boldsymbol{\alpha}^{(2 \times 3)} = [\alpha_1^{(2 \times 3)}, \alpha_2^{(2 \times 3)}, \dots, \alpha_n^{(2 \times 3)}]^T$ and $\boldsymbol{\alpha}^{(1 \times 2 \times 3)} = [\alpha_1^{(1 \times 2 \times 3)}, \alpha_2^{(1 \times 2 \times 3)}, \dots, \alpha_n^{(1 \times 2 \times 3)}]^T$.

Substituting $\mathbf{h}_{\mathbf{M}^{(1)}}$, $\mathbf{h}_{\mathbf{M}^{(2)}}$, $\mathbf{h}_{\mathbf{M}^{(3)}}$, $\mathbf{h}_{\mathbf{M}^{(1)} \times \mathbf{M}^{(2)}}$, $\mathbf{h}_{\mathbf{M}^{(1)} \times \mathbf{M}^{(3)}}$, $\mathbf{h}_{\mathbf{M}^{(2)} \times \mathbf{M}^{(3)}}$ and $\mathbf{h}_{\mathbf{M}^{(1)} \times \mathbf{M}^{(2)} \times \mathbf{M}^{(3)}}$ into Eq. (8),

and applying the reproducing kernel properties, we get

$$\begin{aligned}
\mathcal{L}(\mathbf{y}, \boldsymbol{\beta}, \boldsymbol{\alpha}) &= \frac{1}{2} \boldsymbol{\epsilon}^T \boldsymbol{\epsilon} + \frac{\lambda^{(1)}}{2} [\boldsymbol{\alpha}^{(1)}]^T \mathbf{K}^{(1)} \boldsymbol{\alpha}^{(1)} + \frac{\lambda^{(2)}}{2} [\boldsymbol{\alpha}^{(2)}]^T \mathbf{K}^{(2)} \boldsymbol{\alpha}^{(2)} + \frac{\lambda^{(3)}}{2} [\boldsymbol{\alpha}^{(3)}]^T \mathbf{K}^{(3)} \boldsymbol{\alpha}^{(3)} \\
&+ \frac{\lambda^{(1 \times 2)}}{2} [\boldsymbol{\alpha}^{(1 \times 2)}]^T \mathbf{K}^{(1 \times 2)} \boldsymbol{\alpha}^{(1 \times 2)} + \frac{\lambda^{(1 \times 3)}}{2} [\boldsymbol{\alpha}^{(1 \times 3)}]^T \mathbf{K}^{(1 \times 3)} \boldsymbol{\alpha}^{(1 \times 3)} + \frac{\lambda^{(2 \times 3)}}{2} [\boldsymbol{\alpha}^{(2 \times 3)}]^T \mathbf{K}^{(2 \times 3)} \boldsymbol{\alpha}^{(2 \times 3)} \\
&+ \frac{\lambda^{(1 \times 2 \times 3)}}{2} [\boldsymbol{\alpha}^{(1 \times 2 \times 3)}]^T \mathbf{K}^{(1 \times 2 \times 3)} \boldsymbol{\alpha}^{(1 \times 2 \times 3)}
\end{aligned} \tag{10}$$

where $\boldsymbol{\epsilon} = \mathbf{y} - \mathbf{X}\boldsymbol{\beta} - \mathbf{K}^{(1)}\boldsymbol{\alpha}^{(1)} - \mathbf{K}^{(2)}\boldsymbol{\alpha}^{(2)} - \mathbf{K}^{(3)}\boldsymbol{\alpha}^{(3)} - \mathbf{K}^{(1 \times 2)}\boldsymbol{\alpha}^{(1 \times 2)} - \mathbf{K}^{(1 \times 3)}\boldsymbol{\alpha}^{(1 \times 3)} - \mathbf{K}^{(2 \times 3)}\boldsymbol{\alpha}^{(2 \times 3)} - \mathbf{K}^{(1 \times 2 \times 3)}\boldsymbol{\alpha}^{(1 \times 2 \times 3)}$ and $\boldsymbol{\alpha} = (\boldsymbol{\alpha}^{(1)}, \boldsymbol{\alpha}^{(2)}, \boldsymbol{\alpha}^{(3)}, \boldsymbol{\alpha}^{(1 \times 2)}, \boldsymbol{\alpha}^{(1 \times 3)}, \boldsymbol{\alpha}^{(2 \times 3)}, \boldsymbol{\alpha}^{(1 \times 2 \times 3)})$.

The gradients of \mathcal{L} with respect to the parametric coefficients $\boldsymbol{\beta}$ and nonparametric coefficients $\boldsymbol{\alpha}'$'s are

$$\begin{aligned}
\frac{\partial \mathcal{L}}{\partial \boldsymbol{\beta}} &= \mathbf{X}^T \boldsymbol{\epsilon}, \quad \frac{\partial \mathcal{L}}{\partial \boldsymbol{\alpha}^{(1)}} = [\mathbf{K}^{(1)}]^T \boldsymbol{\epsilon} + \lambda^{(1)} \mathbf{K}^{(1)} \boldsymbol{\alpha}^{(1)}, \\
\frac{\partial \mathcal{L}}{\partial \boldsymbol{\alpha}^{(2)}} &= [\mathbf{K}^{(2)}]^T \boldsymbol{\epsilon} + \lambda^{(2)} \mathbf{K}^{(2)} \boldsymbol{\alpha}^{(2)}, \quad \frac{\partial \mathcal{L}}{\partial \boldsymbol{\alpha}^{(3)}} = [\mathbf{K}^{(3)}]^T \boldsymbol{\epsilon} + \lambda^{(3)} \mathbf{K}^{(3)} \boldsymbol{\alpha}^{(3)}, \\
\frac{\partial \mathcal{L}}{\partial \boldsymbol{\alpha}^{(1 \times 2)}} &= [\mathbf{K}^{(1 \times 2)}]^T \boldsymbol{\epsilon} + \lambda^{(1 \times 2)} \mathbf{K}^{(1 \times 2)} \boldsymbol{\alpha}^{(1 \times 2)}, \quad \frac{\partial \mathcal{L}}{\partial \boldsymbol{\alpha}^{(1 \times 3)}} = [\mathbf{K}^{(1 \times 3)}]^T \boldsymbol{\epsilon} + \lambda^{(1 \times 3)} \mathbf{K}^{(1 \times 3)} \boldsymbol{\alpha}^{(1 \times 3)}, \\
\frac{\partial \mathcal{L}}{\partial \boldsymbol{\alpha}^{(2 \times 3)}} &= [\mathbf{K}^{(2 \times 3)}]^T \boldsymbol{\epsilon} + \lambda^{(2 \times 3)} \mathbf{K}^{(2 \times 3)} \boldsymbol{\alpha}^{(2 \times 3)}, \quad \frac{\partial \mathcal{L}}{\partial \boldsymbol{\alpha}^{(1 \times 2 \times 3)}} = [\mathbf{K}^{(1 \times 2 \times 3)}]^T \boldsymbol{\epsilon} + \lambda^{(1 \times 2 \times 3)} \mathbf{K}^{(1 \times 2 \times 3)} \boldsymbol{\alpha}^{(1 \times 2 \times 3)}
\end{aligned} \tag{11}$$

By setting the gradients to zero, this first-order condition is given by the linear system as follows:

$$\begin{bmatrix}
\mathbf{X}^T \mathbf{X} & \mathbf{X}^T \mathbf{K}^{(1)} & \mathbf{X}^T \mathbf{K}^{(2)} & \mathbf{X}^T \mathbf{K}^{(3)} & \mathbf{X}^T \mathbf{K}^{(1 \times 2)} & \mathbf{X}^T \mathbf{K}^{(1 \times 3)} & \mathbf{X}^T \mathbf{K}^{(2 \times 3)} & \mathbf{X}^T \mathbf{K}^{(1 \times 2 \times 3)} \\
[\mathbf{K}^{(1)}]^T \mathbf{X} & A & [\mathbf{K}^{(1)}]^T \mathbf{K}^{(2)} & [\mathbf{K}^{(1)}]^T \mathbf{K}^{(3)} & [\mathbf{K}^{(1)}]^T \mathbf{K}^{(1 \times 2)} & [\mathbf{K}^{(1)}]^T \mathbf{K}^{(1 \times 3)} & [\mathbf{K}^{(1)}]^T \mathbf{K}^{(2 \times 3)} & [\mathbf{K}^{(1)}]^T \mathbf{K}^{(1 \times 2 \times 3)} \\
[\mathbf{K}^{(2)}]^T \mathbf{X} & [\mathbf{K}^{(2)}]^T \mathbf{K}^{(1)} & B & [\mathbf{K}^{(2)}]^T \mathbf{K}^{(3)} & [\mathbf{K}^{(2)}]^T \mathbf{K}^{(1 \times 2)} & [\mathbf{K}^{(2)}]^T \mathbf{K}^{(1 \times 3)} & [\mathbf{K}^{(2)}]^T \mathbf{K}^{(2 \times 3)} & [\mathbf{K}^{(2)}]^T \mathbf{K}^{(1 \times 2 \times 3)} \\
[\mathbf{K}^{(3)}]^T \mathbf{X} & [\mathbf{K}^{(3)}]^T \mathbf{K}^{(1)} & [\mathbf{K}^{(3)}]^T \mathbf{K}^{(2)} & C & [\mathbf{K}^{(3)}]^T \mathbf{K}^{(1 \times 2)} & [\mathbf{K}^{(3)}]^T \mathbf{K}^{(1 \times 3)} & [\mathbf{K}^{(3)}]^T \mathbf{K}^{(2 \times 3)} & [\mathbf{K}^{(3)}]^T \mathbf{K}^{(1 \times 2 \times 3)} \\
[\mathbf{K}^{(1 \times 2)}]^T \mathbf{X} & [\mathbf{K}^{(1 \times 2)}]^T \mathbf{K}^{(1)} & [\mathbf{K}^{(1 \times 2)}]^T \mathbf{K}^{(2)} & [\mathbf{K}^{(1 \times 2)}]^T \mathbf{K}^{(3)} & D & [\mathbf{K}^{(1 \times 2)}]^T \mathbf{K}^{(1 \times 3)} & [\mathbf{K}^{(1 \times 2)}]^T \mathbf{K}^{(2 \times 3)} & [\mathbf{K}^{(1 \times 2)}]^T \mathbf{K}^{(1 \times 2 \times 3)} \\
[\mathbf{K}^{(1 \times 3)}]^T \mathbf{X} & [\mathbf{K}^{(1 \times 3)}]^T \mathbf{K}^{(1)} & [\mathbf{K}^{(1 \times 3)}]^T \mathbf{K}^{(2)} & [\mathbf{K}^{(1 \times 3)}]^T \mathbf{K}^{(3)} & [\mathbf{K}^{(1 \times 3)}]^T \mathbf{K}^{(1 \times 2)} & E & [\mathbf{K}^{(1 \times 3)}]^T \mathbf{K}^{(2 \times 3)} & [\mathbf{K}^{(1 \times 3)}]^T \mathbf{K}^{(1 \times 2 \times 3)} \\
[\mathbf{K}^{(2 \times 3)}]^T \mathbf{X} & [\mathbf{K}^{(2 \times 3)}]^T \mathbf{K}^{(1)} & [\mathbf{K}^{(2 \times 3)}]^T \mathbf{K}^{(2)} & [\mathbf{K}^{(2 \times 3)}]^T \mathbf{K}^{(3)} & [\mathbf{K}^{(2 \times 3)}]^T \mathbf{K}^{(1 \times 2)} & [\mathbf{K}^{(2 \times 3)}]^T \mathbf{K}^{(1 \times 3)} & F & [\mathbf{K}^{(2 \times 3)}]^T \mathbf{K}^{(1 \times 2 \times 3)} \\
[\mathbf{K}^{(1 \times 2 \times 3)}]^T \mathbf{X} & [\mathbf{K}^{(1 \times 2 \times 3)}]^T \mathbf{K}^{(1)} & [\mathbf{K}^{(1 \times 2 \times 3)}]^T \mathbf{K}^{(2)} & [\mathbf{K}^{(1 \times 2 \times 3)}]^T \mathbf{K}^{(3)} & [\mathbf{K}^{(1 \times 2 \times 3)}]^T \mathbf{K}^{(1 \times 2)} & [\mathbf{K}^{(1 \times 2 \times 3)}]^T \mathbf{K}^{(1 \times 3)} & [\mathbf{K}^{(1 \times 2 \times 3)}]^T \mathbf{K}^{(2 \times 3)} & G
\end{bmatrix}$$

$$\begin{bmatrix}
\boldsymbol{\beta} \\
\boldsymbol{\alpha}^{(1)} \\
\boldsymbol{\alpha}^{(2)} \\
\boldsymbol{\alpha}^{(3)} \\
\boldsymbol{\alpha}^{1 \times 2} \\
\boldsymbol{\alpha}^{1 \times 3} \\
\boldsymbol{\alpha}^{2 \times 3} \\
\boldsymbol{\alpha}^{1 \times 2 \times 3}
\end{bmatrix}
=
\begin{bmatrix}
\mathbf{X}^T \mathbf{y} \\
\mathbf{K}^{(1)} \mathbf{y} \\
\mathbf{K}^{(2)} \mathbf{y} \\
\mathbf{K}^{(3)} \mathbf{y} \\
\mathbf{K}^{(1 \times 2)} \mathbf{y} \\
\mathbf{K}^{(1 \times 3)} \mathbf{y} \\
\mathbf{K}^{(2 \times 3)} \mathbf{y} \\
\mathbf{K}^{(1 \times 2 \times 3)} \mathbf{y}
\end{bmatrix}, \tag{12}$$

where $A = [\mathbf{K}^{(1)}]^T \mathbf{K}^{(1)} + \lambda^{(1)} \mathbf{K}^{(1)}$, $B = [\mathbf{K}^{(2)}]^T \mathbf{K}^{(2)} + \lambda^{(2)} \mathbf{K}^{(2)}$, $C = [\mathbf{K}^{(3)}]^T \mathbf{K}^{(3)} + \lambda^{(3)} \mathbf{K}^{(3)}$, $D = [\mathbf{K}^{(1 \times 2)}]^T \mathbf{K}^{(1 \times 2)} + \lambda^{(1 \times 2)} \mathbf{K}^{(1 \times 2)}$, $E = [\mathbf{K}^{(1 \times 3)}]^T \mathbf{K}^{(1 \times 3)} + \lambda^{(1 \times 3)} \mathbf{K}^{(1 \times 3)}$, $F = [\mathbf{K}^{(2 \times 3)}]^T \mathbf{K}^{(2 \times 3)} + \lambda^{(2 \times 3)} \mathbf{K}^{(2 \times 3)}$, $G = [\mathbf{K}^{(1 \times 2 \times 3)}]^T \mathbf{K}^{(1 \times 2 \times 3)} + \lambda^{(1 \times 2 \times 3)} \mathbf{K}^{(1 \times 2 \times 3)}$. Following many derivations in the literature (e.g., (D. Liu et al., 2007; S. Li & Cui, 2012; Ge et al., 2015)), we can show that a first-order linear

system is equivalent to the normal equation of the linear mixed effects model:

$$\mathbf{y} = \mathbf{X}\boldsymbol{\beta} + \mathbf{h}_{\mathbf{M}(1)} + \mathbf{h}_{\mathbf{M}(2)} + \mathbf{h}_{\mathbf{M}(3)} + \mathbf{h}_{\mathbf{M}(1)\times\mathbf{M}(2)} + \mathbf{h}_{\mathbf{M}(1)\times\mathbf{M}(3)} + \mathbf{h}_{\mathbf{M}(2)\times\mathbf{M}(3)} + \mathbf{h}_{\mathbf{M}(1)\times\mathbf{M}(2)\times\mathbf{M}(3)} + \boldsymbol{\epsilon}, \quad (13)$$

where $\boldsymbol{\beta}$ is a coefficient vector of fixed effects, $\mathbf{h}_{\mathbf{M}(1)}$, $\mathbf{h}_{\mathbf{M}(2)}$, $\mathbf{h}_{\mathbf{M}(3)}$, $\mathbf{h}_{\mathbf{M}(1)\times\mathbf{M}(2)}$, $\mathbf{h}_{\mathbf{M}(1)\times\mathbf{M}(3)}$, $\mathbf{h}_{\mathbf{M}(2)\times\mathbf{M}(3)}$ and $\mathbf{h}_{\mathbf{M}(1)\times\mathbf{M}(2)\times\mathbf{M}(3)}$ are independent random effects with distribution as $\mathbf{h}_{\mathbf{M}(1)} \sim N(0, \tau^{(1)}\mathbf{K}^{(1)})$, $\tau^{(1)} = \frac{\sigma^2}{\lambda^{(1)}}$, $\mathbf{h}_{\mathbf{M}(2)} \sim N(0, \tau^{(2)}\mathbf{K}^{(2)})$, $\tau^{(2)} = \frac{\sigma^2}{\lambda^{(2)}}$, $\mathbf{h}_{\mathbf{M}(3)} \sim N(0, \tau^{(3)}\mathbf{K}^{(3)})$, $\tau^{(3)} = \frac{\sigma^2}{\lambda^{(3)}}$, $\mathbf{h}_{\mathbf{M}(1\times 2)} \sim N(0, \tau^{(1\times 2)}\mathbf{K}^{(1\times 2)})$, $\tau^{(1\times 2)} = \frac{\sigma^2}{\lambda^{(1\times 2)}}$, $\mathbf{h}_{\mathbf{M}(1\times 3)} \sim N(0, \tau^{(1\times 3)}\mathbf{K}^{(1\times 3)})$, $\tau^{(1\times 3)} = \frac{\sigma^2}{\lambda^{(1\times 3)}}$, $\mathbf{h}_{\mathbf{M}(2\times 3)} \sim N(0, \tau^{(2\times 3)}\mathbf{K}^{(2\times 3)})$, $\tau^{(2\times 3)} = \frac{\sigma^2}{\lambda^{(2\times 3)}}$, $\mathbf{h}_{\mathbf{M}(1\times 2\times 3)} \sim N(0, \tau^{(1\times 2\times 3)}\mathbf{K}^{(1\times 2\times 3)})$, $\tau^{(1\times 2\times 3)} = \frac{\sigma^2}{\lambda^{(1\times 2\times 3)}}$. $\boldsymbol{\epsilon}$ is also an independent random variable with the distribution $\boldsymbol{\epsilon} \sim N(0, \sigma^2\mathbf{I})$, where \mathbf{I} is an identity matrix. This relationship insures that all of the effects extracted by minimizing the loss function in Eq. (7), are the same as the best linear unbiased predictors (BLUPs) of the linear mixed effects model in Eq. (13). It is possible to estimate the variance components using the restricted maximum likelihood (ReML) approach (see in the appendix for details). The solution of the linear system in Eq. (12) gives the coefficients of the fixed effect, $\boldsymbol{\beta}$, and coefficients for the random effect, $\boldsymbol{\alpha}$. By inserting $\boldsymbol{\alpha}$ into Eq. (9), we can estimate the random effects $\hat{\mathbf{h}}_{\mathbf{M}(1)}$, $\hat{\mathbf{h}}_{\mathbf{M}(2)}$, $\hat{\mathbf{h}}_{\mathbf{M}(3)}$, $\hat{\mathbf{h}}_{\mathbf{M}(1\times 2)}$, $\hat{\mathbf{h}}_{\mathbf{M}(1\times 3)}$, $\hat{\mathbf{h}}_{\mathbf{M}(2\times 3)}$ and $\hat{\mathbf{h}}_{\mathbf{M}(1\times 2\times 3)}$, respectively.

3 Statistical testing

Using positive definite kernels, we treat each gene-derived SNP, ROI, and gene-derived DNA methylation as a testing unit. In the following subsections, we study the test statistic of the overall effect and higher order interaction effects.

3.1 Testing overall effect

We know that the overall testing effect $H_0 : h_{\mathbf{M}(1)}(\cdot) = h_{\mathbf{M}(2)}(\cdot) = h_{\mathbf{M}(3)}(\cdot) = h_{\mathbf{M}(1)\times\mathbf{M}(2)}(\cdot) = h_{\mathbf{M}(1)\times\mathbf{M}(3)}(\cdot) = h_{\mathbf{M}(2)\times\mathbf{M}(3)}(\cdot) = h_{\mathbf{M}(1)\times\mathbf{M}(2)\times\mathbf{M}(3)}(\cdot) = 0$ is equivalent to test the variance components in Eq.(13), $H_0 : \tau^{(1)} = \tau^{(2)} = \tau^{(3)} = \tau^{(1\times 2)} = \tau^{(1\times 3)} = \tau^{(2\times 3)} = \tau^{(1\times 2\times 3)} = 0$.

Unfortunately, under the null hypothesis, the asymptotic distribution of a likelihood ratio test (LRT) statistic does not follow a chi-square distribution or a mixture chi-square distribution. Because the parameters in the variance components analysis are laid on the boundary of the parameter space when the null hypothesis is true and kernel matrices are not block-diagonal, S. Li and Cui (2012) have proposed a score test statistic based on the restricted likelihood. In this paper, we have constructed a score test statistic for the multi-view data model, Eq. (13). Assuming that the linear mixed model in Eq. (13) has multivariate normal distribution with mean $\mathbf{X}\boldsymbol{\beta}$ and variance-

covariance matrix $\Theta(\theta) = \sigma^2 \mathbf{I} + \tau^{(1)} \mathbf{K}^{(1)} + \tau^{(2)} \mathbf{K}^{(2)} + \tau^{(3)} \mathbf{K}^{(3)} + \tau^{(1 \times 2)} \mathbf{K}^{(1 \times 2)} + \tau^{(1 \times 3)} \mathbf{K}^{(1 \times 3)} + \tau^{(2 \times 3)} \mathbf{K}^{(2 \times 3)} + \tau^{(1 \times 2 \times 3)} \mathbf{K}^{(1 \times 2 \times 3)}$, where $\theta = (\sigma^2, \tau^{(1)}, \tau^{(2)}, \tau^{(3)}, \tau^{(1 \times 2)}, \tau^{(2 \times 3)}, \tau^{(1 \times 2 \times 3)})$ are the variance components.

The restricted log-likelihood function of Eq. (13) can be written as

$$\ell_R(\theta) = -\frac{1}{2} \ln(|\Theta(\theta)|) - \frac{1}{2} \ln(|\mathbf{X}^T \Theta^{-1}(\theta) \mathbf{X}|) - \frac{1}{2} (\mathbf{y} - \mathbf{X}\hat{\boldsymbol{\beta}})^T \Theta^{-1}(\theta) (\mathbf{y} - \mathbf{X}\hat{\boldsymbol{\beta}}) \quad (14)$$

The estimate of the variance components are obtained by the partial derivative of Eq. (14) with respect to each of the variance components (see appendix for more detail). By considering that the true value of σ^2 under the null hypothesis is σ_0^2 , under the ReML the score test statistic is defined as

$$S(\sigma_0^2) = \frac{1}{2\sigma_0^2} (\mathbf{y} - \mathbf{X}\hat{\boldsymbol{\beta}})^T \mathbf{K} (\mathbf{y} - \mathbf{X}\hat{\boldsymbol{\beta}}) \quad (15)$$

where $\mathbf{K} = \mathbf{K}^{(1)} + \mathbf{K}^{(2)} + \mathbf{K}^{(3)} + \mathbf{K}^{(1 \times 2)} + \mathbf{K}^{(1 \times 3)} + \mathbf{K}^{(2 \times 3)} + \mathbf{K}^{(1 \times 2 \times 3)}$, $\hat{\boldsymbol{\beta}}$ is the maximum likelihood estimator (MLE) of the regression coefficient under the null hypothesis $\mathbf{y} = \mathbf{X}\boldsymbol{\beta} + \epsilon_0$, σ_0^2 is the variance of ϵ_0 , and $S(\sigma_0^2)$ is the quadratic function for the variable \mathbf{y} , which follows a mixture of the chi-square distribution under the null hypothesis. By the Satterthwaite method (Satterthwaite, 1946), we can approximate the distribution of $S(\sigma_0^2)$ to a scaled chi-square distribution, i.e., $S(\sigma_0^2) \sim \gamma \chi_\nu^2$, where the scale parameter γ and the degrees of freedom ν can be measured by the method of moments (MOM). The mean and variance of the test statistic $S(\sigma_0^2)$ are

$$E[S(\sigma_0^2)] = E[\gamma \chi_\nu^2] = \gamma \nu, \quad \text{and} \quad \text{Var}[S(\sigma_0^2)] = \text{Var}[\gamma \chi_\nu^2] = 2\gamma^2 \nu,$$

respectively. By solving the above two equations, we have $\hat{\gamma} = \frac{\text{Var}[S(\sigma_0^2)]}{2E[S(\sigma_0^2)]}$ and $\hat{\nu} = \frac{2E[S(\sigma_0^2)]^2}{\text{Var}[S(\sigma_0^2)]}$. In practices, σ_0^2 is unknown but we can replace it by its ReML under the null model denoted by $\hat{\sigma}_0^2$. Lastly, the p -value of an experimental score statistic $S(\hat{\sigma}_0^2)$ is obtained using the scaled chi-square distribution $\hat{\gamma} \chi_{\hat{\nu}}^2$.

3.2 Testing higher order interaction effect

To test the higher order interaction effect, we show that testing the null hypothesis $H_0 : h_{\mathbf{M}^{(1)} \times \mathbf{M}^{(2)} \times \mathbf{M}^{(3)}}(\cdot) = 0$ is equivalent to testing the variance component: $H_0 : \tau^{(1 \times 2 \times 3)} = 0$. Let $\Sigma = \sigma^2 \mathbf{I} + \tau^{(1)} \mathbf{K}^{(1)} + \tau^{(2)} \mathbf{K}^{(2)} + \tau^{(3)} \mathbf{K}^{(3)} + \tau^{1 \times 2} \mathbf{K}^{(1 \times 2)} + \tau^{1 \times 3} \mathbf{K}^{(1 \times 3)} + \tau^{2 \times 3} \mathbf{K}^{(2 \times 3)}$, and $\tau^{(1)}, \tau^{(2)}, \tau^{(3)}, \tau^{(1 \times 2)}, \tau^{(1 \times 3)}, \tau^{(2 \times 3)}$, and σ^2 are model parameters under the null model $\mathbf{y} = \mathbf{X}\boldsymbol{\beta} + \mathbf{h}_{\mathbf{M}^{(1)}} + \mathbf{h}_{\mathbf{M}^{(2)}} + \mathbf{h}_{\mathbf{M}^{(3)}} + \mathbf{h}_{\mathbf{M}^{(1)} \times \mathbf{M}^{(2)}} + \mathbf{h}_{\mathbf{M}^{(1)} \times \mathbf{M}^{(3)}} + \boldsymbol{\epsilon}$.

We formulate a test statistic:

$$S_I(\boldsymbol{\tau}_I) = \frac{1}{2\sigma_0^2} \mathbf{y}^T \mathbf{W}_{01} \mathbf{K}^{(1 \times 2 \times 3)} \mathbf{W}_{01} \mathbf{y}, \quad (16)$$

where $\boldsymbol{\tau}_I = (\sigma^2, \tau^{(1)}, \tau^{(2)}, \tau^{(3)}, \tau^{(1 \times 2)}, \tau^{(1 \times 3)}, \tau^{(2 \times 3)})$, and $\mathbf{W}_{01} = \boldsymbol{\Sigma}^{-1} - \boldsymbol{\Sigma}^{-1} \mathbf{X} (\mathbf{X}^T \boldsymbol{\Sigma}^{-1} \mathbf{X})^{-1} \mathbf{X}^T \boldsymbol{\Sigma}^{-1}$ is the projection matrix under the null hypothesis. Similarly to the overall effect test, we can use the Satterthwaite method to approximate the distribution for the higher order intersection test statistic $S_I(\boldsymbol{\tau}_I)$ by a scaled chi-square distribution with scaled γ_I and degree of freedom ν_I , i.e., $S_I(\boldsymbol{\tau}_I) \sim \gamma_I \chi_{\nu_I}^2$. The scaled parameter and degree of freedom are estimated by the MOM, $\hat{\gamma}_I = \frac{\text{Var}[S_I(\boldsymbol{\tau}_I)]}{2\text{E}[S_I(\boldsymbol{\tau}_I)]}$ and $\hat{\nu}_I = \frac{2\text{E}[S_I(\boldsymbol{\tau}_I)]}{\text{Var}[S_I(\boldsymbol{\tau}_I)]}$, respectively. In practice, the unknown model parameters $\tau^{(1)}, \tau^{(2)}, \tau^{(3)}, \tau^{(1 \times 2)}, \tau^{(1 \times 3)}, \tau^{(2 \times 3)}$, and σ^2 are estimated by their respective ReML estimates $\hat{\tau}^{(1)}, \hat{\tau}^{(2)}, \hat{\tau}^{(3)}, \hat{\tau}^{(1 \times 2)}, \hat{\tau}^{(1 \times 3)}, \hat{\tau}^{(2 \times 3)}$, and $\hat{\sigma}^2$ under the null hypothesis. Lastly, the p -value for the observed higher order interaction effect (score statistic $S_I(\boldsymbol{\tau}_I)$) is obtained using the scaled chi-square distribution $\hat{\gamma}_I \chi_{\hat{\nu}_I}^2$.

3.3 Kernel choice

In kernel methods, choosing a suitable kernel is indispensable. Most kernel methods suffer from poor selection of a suitable kernel. It is often the case that the kernel has parameters which may strongly influence the results. Assuming $k : \mathcal{X} \times \mathcal{X} \rightarrow \mathbb{R}$ is a positive definite kernel. Then for any $X, \tilde{X} \in \mathcal{X}$, a linear positive definite kernels on \mathbb{R} is defined as

$$k(X, \tilde{X}) = \langle X, \tilde{X} \rangle = X^T \tilde{X}.$$

The linear kernel is used by the underlying Euclidean space to define the similarity measure. Whenever the dimensionality of \mathbf{X} is very high, this may allow for more complexity in the function class than what we could measure and assess otherwise. The polynomial kernel is defined as

$$k(X, \tilde{X}) = (X^T \tilde{X} + c)^d, \quad (c \geq 0, d \in \mathbb{N}).$$

Using the polynomial kernel makes it possible to use higher order correlations between data for different purposes. This kernel incorporates every polynomial interaction up to degree d (provided that $c > 0$). For instance, if we want to take only the mean and variance into account, we only need to consider $d = 2$ and $c = 1$. For more emphasis on mean we need to increase the constant offset a . Polynomial kernels only map data into a finite dimensional space. Due to the finite bounded degree the given kernel will not provide us with guarantees for a good dependency measure. In addition,

both linear and polynomial kernels are unbounded.

Many radial basis function kernels, such as the Gaussian kernel, map X into a infinite dimensional space. The Gaussian kernel is defined as:

$$k(X, \tilde{X}) = e^{\frac{1}{2\sigma^2} - \|X - \tilde{X}\|^2}, (\sigma > 0).$$

While the Gaussian kernel has a free parameter (bandwidth), it still follows a number of theoretical properties such as boundedness, consistence, universality, robustness etc. It is the most applicable kernel of the kernel methods (B. K. Sriperumbudur & Schölkopf, 2009). For the Gaussian kernel, we can use the median of the pairwise distance as a bandwidth (Gretton et al., 2008; Song, Smola, Gretton, Bedo, & Borgwardt, 2012).

For GWASs, a kernel captures the pairwise similarity across a number of SNPs in each gene. Kernel projects the genotype data from original space (high dimension and nonlinear) to a feature space (linear space). One of the more popular kernels used for genomics similarity is the identity-by-state (IBS) kernel (nonparametric function of the genotypes) (L. C. Kwee, 2008):

$$k(\mathbf{M}_i, \mathbf{M}_j) = 1 - \frac{1}{2s} \sum_{b=1}^s |M_{ib} - M_{jb}|.$$

where s is the number of SNP markers of the corresponding gene. The IBS kernel does not need any assumption on these types of genetic interactions. Thus, in principle, it can capture any effect between genetic features and their influences on the phenotype. In this paper, we used the Gaussian kernel for the quantitative data view (imaging and epigenetics) and the IBS kernel for the qualitative data view (genetics).

4 Relevant methods

Li and Cui (2012) have proposed a linear PCA (LPCA) based regression method for the interaction effect between two genes. This makes it possible to extend the notion to three datasets. Let $\mathbf{M}^{(1)} = [M_1^1, M_2^1, \dots, M_s^1]$, $\mathbf{M}^{(2)} = [M_1^2, M_2^2, \dots, M_r^2]$, and $\mathbf{M}^{(3)} = [M_1^3, M_2^3, \dots, M_d^3]$ be the data matrix for the genetics, imaging and epigenetics, respectively. Using the PCA we can compute the first ℓ principle components: $U_1^1, U_2^1, \dots, U_{s_\ell}^1$, $U_1^2, U_2^2, \dots, U_{r_\ell}^2$, and $U_1^3, U_2^3, \dots, U_{d_\ell}^3$ with $s_\ell \leq s$, $r_\ell \leq r$, and $d_\ell \leq d$, for the corresponding data matrix, respectively. We then compared the numerical, simulation and real data analysis with the following methods: test based on only first and first few principal components multiple regression, which we are called partial principal component

regression (pPCAR) and full principal component regression (fPCAR)), respectively.

4.1 Principal component multiple regression

By considering only the first principal component, the 3rd order interaction model (i.e., pPCA) can be stated as:

$$\mathbf{y} = \mathbf{X}\boldsymbol{\beta} + \sum_{a=1}^s \alpha_a \mathbf{M}_a^{(1)} + \sum_{b=1}^r \alpha_b \mathbf{M}_b^{(2)} + \sum_{c=1}^d \alpha_c \mathbf{M}_c^{(3)} + \eta U_1^{(1)} U_1^{(2)} U_1^{(3)}. \quad (17)$$

This model is called partial PCA regression (pPCAR). Using the multiple regression in Eq. (17), the interaction of $\mathbf{M}^{(1)} \times \mathbf{M}^{(2)} \times \mathbf{M}^{(3)}$ is assessed by testing $H_0 : \eta = 0$. To consider all possible interactions of the selected principal components, we can also replace the main effects by the first ℓ principal components. The number of principal components ℓ is selected based on the proportion of variation explained by the principal components, which can explain the major variations (say, $\geq 85\%$). The models in Eq. (17) then becomes

$$\mathbf{y} = \mathbf{X}\boldsymbol{\beta} + \sum_{a=1}^{s_\ell} \alpha_a U_a^{(1)} + \sum_{b=1}^{r_\ell} \alpha_b U_b^{(2)} + \sum_{c=1}^{d_\ell} \alpha_c U_c^{(3)} + \sum_{a=1}^{s_\ell} \sum_{b=1}^{r_\ell} \sum_{c=1}^{d_\ell} \eta_{123} U_a^{(1)} U_b^{(2)} U_c^{(3)} \quad (18)$$

Using the multiple regression in Eq. (18), the interaction of $\mathbf{M}^{(1)} \times \mathbf{M}^{(2)} \times \mathbf{M}^{(3)}$ is assessed by testing $H_0 : \eta_{123} = 0$.

4.2 Principal component sequence kernel association test

Over the past several years, the sequence kernel association test (SKAT) approach has been widely used in GWASs due to its flexibility and computational efficiency. The SKAT is based on a SNP-set (e.g., a gene or a region) level test for the association between a set of variants and dichotomous or quantitative phenotypes. This method aggregates individual test statistics of SNPs and efficiently computes SNP-set level p-values, while adjusting for covariates, such as principal components to account for population stratification (M. C. Wu et al., 2011; I. Ionita-Laza, 2013). We applied SKAT to gene-derived SNPs, ROIs, and gene-derived DNA methylations data. To do this, we use SKAT in Eq. (18) and the interaction of $\mathbf{M}^{(1)} \times \mathbf{M}^{(2)} \times \mathbf{M}^{(3)}$ is assessed by testing $H_0 : \eta_{123} = 0$.

5 Experiments

We conducted experiments on both the simulation studies (numerical data and real MCIC data) and imaging genetics with the SZ study. We considered the IBS kernel for the genetic data and the Gaussian kernel for all other data. For the Gaussian kernel, we used the median of the pairwise distance as the bandwidth. The proposed method is based on the ReML algorithm (Fisher's scoring algorithm). The ReML algorithm converged in less than 50 iterations (the difference between successive log ReML values was smaller than 10^{-04}), and in most of the cases it converged very quickly with 10 iterations, taking only a few seconds with an R-program. Solving the ReML may be trapped by local minima. To avoid this problem, we use a set of initial points (0, 0.00001, 0.0001, 0.001, 0.01, 0.1, 1) for the optimization algorithm and chose the best one (maximized ReML).

5.1 Simulation studies

The goal of these simulation studies is to evaluate the performance of the proposed method and the accuracy of the score tests. To synthesize quantitative phenotypes, we applied the following model:

$$y_i = \mathbf{X}_i^T \beta + \alpha_1 [h_S(S_i) + h_T(T_i) + h_C(C_i)] + \alpha_2 [h_{S \times T}(S_i, T_i) + h_{S \times C}(S_i, C_i) + h_{T \times C}(T_i, C_i)] + \alpha_3 [h_{S \times T \times C}(S_i, T_i, C_i)] + \sigma \epsilon_i \quad (19)$$

where \mathbf{X}_i is a vector of covariates including an intercept (e.g., age, height, etc.,) of i th subject ($i = 1, 2, \dots, n$) and β 's are the coefficient. S_i , T_i , and C_i are the three data sets and ϵ_i is a random error that follows the Gaussian distribution with mean zero and unit variance, i.e., $\epsilon_i \sim N(0, 1)$, and σ is the standard deviation of the error and was fixed to 10^{-02} , of the i -th subject. For each function, we designed the following form

$$h_S(S_i) = \sum_{a=1}^{10} S[i, a] \cos(S[i, a]), \quad h_T(T_i) = \sum_{b=1}^2 2T[i, b] \sin(T[i, b]), \quad h_C(C_i) = \sum_{c=1}^{10} \frac{i}{\sqrt{2} \exp(C[i, c])},$$

$$h_{S \times T}(S_i, T_i) = h_S(S_i) 2h_T(T_i), \quad h_{S \times C}(S_i, C_i) = h_S(S_i) 3h_C(C_i), \quad h_{T \times C}(S_i, T_i) = 2h_T(T_i) 3h_C(C_i),$$

$$h_{S \times T \times C}(S_i, T_i, C_i) = h_S(S_i) 2h_T(T_i) 3h_C(C_i).$$

In simulation-I and simulation-II, we generated data under different values of $(\alpha_1, \alpha_2, \alpha_3)$ to evaluate the performance of the test. In other words, for $\alpha_1 = \alpha_2 = \alpha_3 = 0$ both main effects and all interaction effects vanish and we examined the false positive rate of the score test of the over all effect. For $\alpha_1 \geq 0, \alpha_2 = 0$ ($\alpha_2 \geq 0$) and $\alpha_3 = 0$, there are main effects (2nd order interaction effects) but no higher order interaction effects, hence we can evaluate the power of the score test. We also set $(\alpha_1, \alpha_2, \alpha_3)$ to many different values to test the power of both score tests. In each setting 500

simulations were performed to confirm the variation of the results.

5.1.1 Simulation-I (numerical data)

In this simulation, we generated two covariates (height and weight) and three views (genetics, topological, and categorical data). We generated the height and weight by the regular sequencing of the interval (50, 80) and (60, 225) with increment of 2.05 and 4.7 for the $n = 500$ subject, respectively. Then, we added the noise $3N(0, 1)$ to each of the variables. The element of coefficient vector β is fixed to 0.5. For the genetics data, we simulated a gene with 10 SNPs using the latent model for 500 subjects as in (Parkhomenko, Tritchler, & Beyene, 2009; Alam, Komori, et al., 2016). We generated data along three circles of different radii with small noise for topological features (Alam & Fukumizu, 2014):

$$T_i = r_i \begin{pmatrix} \cos(\mathbf{R}_i) \\ \sin(\mathbf{R}_i) \end{pmatrix} + \epsilon_i,$$

where $r_i = 1, 0.5$ and 0.25 , for $i = 1, \dots, n_1$, $i = n_1 + 1, \dots, n_2$, and $i = n_2 + 1, \dots, n_3$ ($n = n_1 + n_2 + n_3 = 500$), respectively, $\mathbf{R}_i \sim U[-1, 1]$ and $\epsilon_i \sim \mathcal{N}(0, I_2)$ independently. For the categorical data, we considered 10 categories with probability $1/10$ and converted these features into the dummy features with levels zero and one.

In addition, to draw the receiver operating characteristic (ROC) the data was generated by fixing $\alpha_1 = 1$, $\alpha_2 = 1$ and α_3 was allocated with probability 0.5 for each run, whether a random number was uniformly distributed on $[0, 1]$ or at 0. We also only fixed $\alpha_1 = 1$ and for each run α_3 ($\alpha_2 = \alpha_3$) was allocated with probability 0.5, whether a random number is uniformly distributed on $[0, 1]$ or at 0. We considered three sample sizes $n \in \{100, 500, 1000\}$ and compared the ROC curves of the proposed method with the three state-of-the-art methods in identifying the interaction effects.

5.2 Simulation-II (Mind Clinical Imaging Consortium's schizophrenia data)

To validate Eq. (19) under different values of $(\alpha_1, \alpha_2, \alpha_3)$, we consider real data. This simulation was based on the SZ data which was collected by the MCIC (J. Chen et al., 2012; J. Liu et al., 2014; Chekouo et al., 2016). These are 208 subjects including 92 schizophrenic patients (age: 34 ± 11 , 22 females) and 116 (age: 32 ± 11 , 44 females) healthy controls. All participants' symptoms were evaluated by the scale for the assessment of positive symptoms and negative symptoms (Andreasen, 1984). By filtering missing data, the number of subjects was reduced to 182 subjects (79 SZ patients

and 103 healthy controls). We considered the age, height, and weight as the covariates and gene-derived SNP, ROIs with voxels, and gene-derived DNA methylation information as the three views.

Genetics: For each subject (SZ patients and healthy controls) a blood sample was taken and DNA was extracted. Gene typing was performed for all subjects at the Mind Research Network using the Illumina Infinium HumanOmni1-Quad assay covering 1140419 SNP loci. To form the final genotype calls and to perform a series of standard quality control procedures the bead studio and PLINK software packages were applied, respectively. The final dataset spans 722177 loci with 22442 genes of 182 subjects. Genotypes “aa” (non-minor allele), “Aa” (one minor allele) and “AA” (two minor alleles) were coded as 0, 1 and 2 for each SNP, respectively (Alam, Komori, et al., 2016). A list of the top 75 genes for the SZ are listed in the SZ genes database (<https://bioinfo.uth.edu/SZGR/>).

Imaging: Participants’ fMRI data were collected during a block design motor response for auditory stimulation. State-of-the-art approaches using participant feedback and expert observation were used. The aim was to continuously monitor the patients while acquiring images with the parameters (TR=2000 ms, TE= 30ms, field of view=22cm, slice thickness=4mm, 1 mm skip, 27 slices, acquisition matrix 64×64 , flip angle=90°) on a Siemens 3T Trio Scanner and 1.5 T Sonata. The data comes from four different sites (& scanners) with echo-planar imaging (EPI). Data were pre-processed with SPM software and were realigned spatially, normalized and resliced to $3 \times 3 \times 3$ mm. They were smoothed with a $10 \times 10 \times 10$ mm³ Gaussian kernel and then analyzed by multiple regression that considered the stimulus and their temporal derivatives plus an intercept term as a regressors. Finally the stimulus-on versus stimulus-off contrast images were extracted. Next, 41236 voxels were extracted from 116 ROIs based on the AAL brain atlas for analysis (Alam, Calhoun, & Wang, 2016). For imaging features (ROIs), we considered 116 ROIs. The name for the ROIs is given by the automated anatomical labeling (AAL) template (Yan & Zang, 2010).

Epigenetics: DNA methylation is one of the main epigenetic mechanisms to regulate gene expression, and may be involved in the development of SZ. For this paper, we investigated 27481 DNA methylation markers in blood from SZ patients and healthy controls. DNA from blood samples were measured by the Illumina Infinium Methylation27 Assay. The methylation value is calculated by taking the ratio of the methylated probe intensity and the total probe intensity.

In this paper, the top 72 genes (from <https://bioinfo.uth.edu/SZGR/> and genes have more than one SNP), 116 ROIs, and from DNA methylation 129 genes (genes have more than 5 methylations) are considered as gene-derived SNPs, ROIs with voxel, and gene-derived DNA methylations features, respectively.

5.3 Simulation results

Table 1 presents the simulation results (simulation-I and simulation-II) for the overall and higher order interaction tests. The nominal p -value threshold was fixed to 0.05. By observing this table, we can see that when $\alpha_1 = \alpha_2 = \alpha_3 = 0$, the size of the overall score test is close to the nominal p -value threshold. When $\alpha_1 \geq 0$, $\alpha_2 = 0$ (or $(\alpha_2 \geq 0)$) and $\alpha_3 = 0$, the false positive rate of the test for higher order interaction effects is also controlled. For the power analysis ($\alpha_3 \geq 0$) we found that the power of the interaction test for the proposed method quickly exceeds 0.85 and 0.90 for simulation-I and simulation-II, respectively. While the SKAT method has higher power when compared to other relevant methods (pPCAR and fPCA) it has lower power when compared to the proposed method both in simulation-I and in simulation-II. We observed that dimension reduction methods (pPCAR and fPCA) can significantly inflate the false positive rates and dramatically loses power when compared to the proposed one and SKAT methods.

Figure 2 shows the receiver operating characteristics (ROC) of the proposed method and three alternative methods to detect interactions using the simulation-III with three sample sizes, $n \in \{100, 500, 1000\}$ for (a) third parameter value is random only, (b) second and third parameter values are random. The sensitivity are plotted against (1- specificity) with the p -values threshold in the range 0 – 1 with a step size 0.0001. The power gain of the proposed method relative to the alternative methods is evident in all situations. When the sample size was increased, and the second order interaction was equal to one, a higher power was observed. We also observed extremely high power for the similar second and higher order interactions.

5.4 Application to imaging genetics and epigenetics with schizophrenia

Here it is demonstrated the power of our proposed method and SKAT utilization for imaging genetic and epigenetic SZ data collected by MCIC. The key to integration, here, is to characterize the underlying interactions between the genetic features (gene-derived SNPs), human brain features (ROIs) and epigenetic features (gene-derived DNA methylation) with covariates (age, height, weight) on hippocampal volume derived from structural MRI scans of the SZ. To do this, we extracted significant (gene-derived SNPs)-ROI-(gene-derived DNA methylations) interactions using the proposed method and compared them to the SKAT methods.

By considering 72 genes-derived SNP, 116 ROIs and 129 gene-derived DNA methylation, we have 1077408 ($72 \times 116 \times 129$) triplets. By the overall tests, we obtained 15436 significant triplets at a 5% level ($p \leq 0.05$). Figure 3 visualizes the index plot of $-\log_{10}(p)$ for 15436 triplets (the triplets in X-axis and $-\log_{10}(p)$ in Y-axis). The vertical solid, dotted and double dotted lines indicate the

Table 1: Power of the overall and higher order interaction score tests, and the alternative methods for interaction detection based on dimension reduction regression (pPCAR, fPCAR) and sequence kernel association test (SKAT). The nominal p -values threshold was fixed to 0.05.

Parameters $(\alpha_1, \alpha_2, \alpha_3)$	Simulation - I					Simulation-II				
	KMDHOI		State-of-the-art methods			KMDHOI		State-of-the-art methods		
	Overall	HOI	pPCAR HOI	fPCAR HOI	SKAT HOI	Overall	HOI	pPCAR HOI	fPCAR HOI	SKAT HOI
(0, 0, 0)	0.047	0.003	0.044	0.036	0.052	0.055	0.009	0.046	0.056	0.045
(0.5, 0, 0)	1.00	0.000	0.137	0.041	0.127	0.999	0.339	0.172	0.077	0.188
(1, 0, 0)	1.00	0.000	0.060	0.015	0.143	0.999	0.457	0.199	0.077	0.176
(0, 0.5, 0)	1.00	0.336	0.137	0.053	0.160	1.000	0.882	0.189	0.095	0.261
(0, 0.5, 0.5)	1.00	0.745	0.161	0.093	0.410	1.000	0.899	0.199	0.107	0.288
(0, 0.5, 1)	1.00	0.843	0.157	0.082	0.478	1.000	0.904	0.173	0.092	0.305
(0, 0, 0.1)	1.00	0.813	0.173	0.080	0.787	1.000	0.924	0.231	0.132	0.362
(0, 0, 1)	1.00	0.882	0.213	0.110	0.748	1.000	0.918	0.283	0.115	0.351
(0.5, 0.5, 0.5)	1.00	0.765	0.174	0.107	0.403	1.000	0.872	0.151	0.117	0.381
(1, 1, 1)	1.00	0.785	0.207	0.111	0.526	1.000	0.896	0.190	0.110	0.405

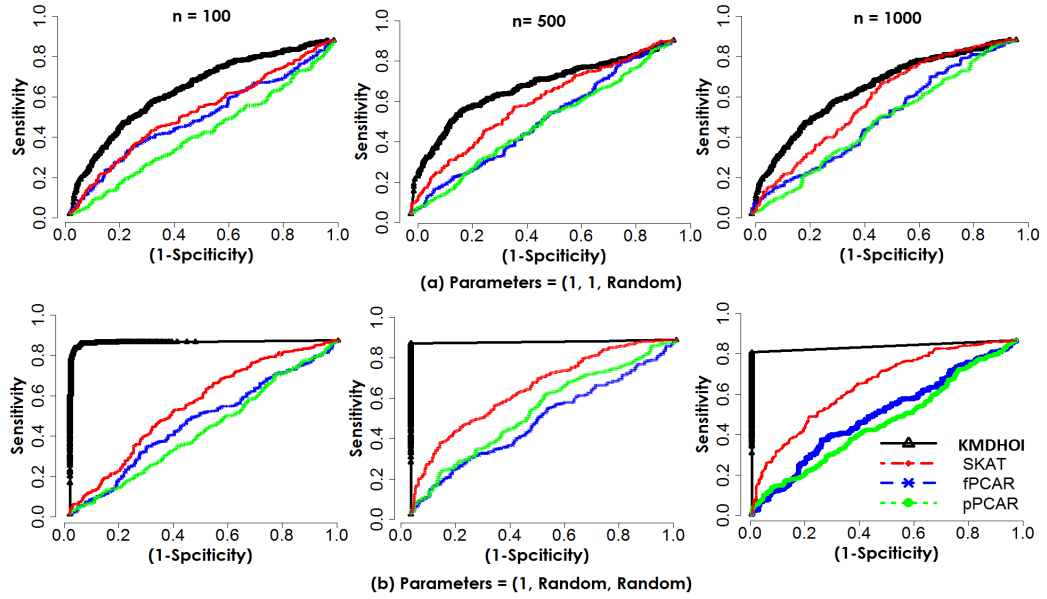


Figure 2: Receiver operating characteristics (ROC) of the kernel methods and relevant methods for higher order interaction detection with three sample sizes, $n \in \{100, 500, 1000\}$ for (a) third parameter value is random, (b) second and third parameter values are random. The sensitivity are plotted against (1- specificity) with the p -values threshold in the range zero to one ($0 - 1$) with a step size 0.0001.

p-values at 0.05, 0.01, 0.001, respectively. Based on these lines, we observed that 272, 72, and 13 triplets are identified to have significantly higher order interactions at 0.05, 0.01 and 0.001 levels, respectively.

Table 2 presents the ReML estimates of σ^2 , $\tau^{(1)}$, $\tau^{(2)}$, $\tau^{(3)}$, $\tau^{(1 \times 2)}$, $\tau^{(1 \times 3)}$, $\tau^{(2 \times 3)}$, $\tau^{(1 \times 2 \times 3)}$ and the p -values for the proposed and SKAT methods on each of the 13 triplets, which are identified to have interaction significance at a level of 0.001. At this p -value, we have 6 gene-derived SNPs (**IL1B**, **MAGI2**, **NRG1**, **PDLIM5**, **SLC18A1**, **TDRD3**), 10 ROIs (**CRBL8.L**, **CRBLCrus1.L**, **ORB-SUP.R**, **LING.L**, **CAU.R**, **IPL.L**, **IPL.R**, **PoCG.L**, **ITG.R**, **VER54**), and 6 gene-derived DNA methylations (**CRABP1**, **FBXO28**, **DUSP1**, **FHIT**, **PLAGL1**, **TFPI2**) that have significant interaction effects on the hippocampal volume of SZ patients.

Figure 4 shows the network within each genetics, imaging and epigenetics interactions as well as the interactions they have between all others views. Each node represents the gene-derived SNPs, ROIs and gene-derived DNA methylations, respectively. The interacting genes-derived SNPs, ROIs and gene-derived DNA methylations are connected with lines. The thickness of the connection line indicates the strength of the interaction among genes-derived SNPs, ROIs and gene-derived DNA methylations. These selected gene-derived SNPs and gene-derived DNA methylations show the interactions between several other genes. The selected ROIs also show the interaction within each selected ROI (shown in Figure 4) as well as the other ROIs (not shown in the figure). Following many studies in the literature, we have shown that each selected gene-derived SNPs our method has identified also has robust research discussing its role in the expression of SZ disease (Siawa, Liuc, Linc, Beend, & Hsiehc, 2016; Shibuya et al., 2013; Koide, Banno, Aleksic, & et al., 2013; Harrison & Law, 206; Moselhy, Eapenb, Akawi, Younis, & et. al., 2015; Bly, 2005).

Recent research has also shown that the 10 ROIs selected by the proposed method have a critical role in brain related diseases (Suk, Wee, Lee, & Shen, 2016; Z. Chen, Liu, Gross, & Beaulieu, 2013; K. Wu et al., 2013). We additionally investigated the 10 ROIs to confirm their role in SZ. To do this, each multidimensional variable ROI was converted to a univariate variable by taking the weighted mean. We then evaluated the differences between the SZ candidates and healthy controls using network measures and visualizations. Table 3 presents the transitivity, degree and global efficiency of each ROI for the SZ candidate and network and healthy control. From this table, we observed that the transitivity (measuring the probability that the adjacent vertices of a vertex are connected) of the SZ candidate group is larger than in the healthy control group (most of the ROIs and on average); this suggests that SZ tends to have more transitive triples. The degree (the number of edges incident to the vertex) of the SZ candidate group is larger than in the healthy control group

for all of the ROIs; this indicates that these ROIs could have an impact on the SZ candidate. The global efficiency, the mean of all nodal efficiencies, of the SZ candidate group is different from the healthy control group. This may suggest that functional activity of the SZ candidate is not similar to the functional activity of the healthy control group in these regions. Figure 5 shows the visualization of correlation matrices, axial view with all networks and networks with correlation > 0.05 for the SZ candidate and healthy control group. From Figure 5, it can be observed that the ROIs in the SZ candidate groups are more correlated and connected than the healthy control group. Therefore, with strong agreement, it has been shown that the selected ROIs have potential impact on the expression of SZ disease.

Table 4 lists the selected significant gene-derived SNP, ROIs and gene-derived DNA methylation using the proposed method (KMDHOI) and SKAT at a $p \leq 0.01$. We found that 31 gene-derived SNP, 35 ROIs and 20 genes-derived DNA methylation from 72 triplets were identified to have significance on the hippocampal volume of the SZ patients and the healthy controls. We also observed that 6 gene-derived SNPs, 10 ROIs and 6 gene-derived DNA methylations were significant at a $p \leq 0.001$. The underlined elements indicated in Table 4 have significant interaction triplets. Table 5 & 6 (in the appendix) lists 72 triplets, which were significant at a $p \leq 0.001$.

For the proposed KMDHOI approach, we considered triplets (gene-derived SNP, ROI, gene-derived DNA methylation) with a $p \leq 4^{-8}$ to be statistically significant after the Bonferroni correction for 1077408 tests. Although the interaction (gene-derived SNP, ROI, gene-derived DNA methylation) results do not appear to be significant after adjusting for multiple comparisons, some of them appear promising consistent results. According to the p -values, we can determine the gene-derived SNPs, ROIs, and gene-derived DNA methylations that have a highly significant hippocampal volume on SZ patients and healthy controls. We observed gene-derived SNP (**MAGI2**, **NRG1**, **SLC18A1**, **TDRD3**), ROIs (**CRBL8.L**, **CRBLCrus1.L**, **ORBSUP.R**, **LING.L**, **IPL.L**, **IPL.R**) and gene-derived DNA methylations (**CRABP1**, **FBXO28**, **FHIT**, **PLAGL1**) at a $p \leq 0.0001$, gene-derived SNP (**MAGI2**, **NRG1**, **TDRD3**), ROIs (**CRBL8.L**, **CRBLCrus1.L**, **IPL.L**, **IPL.R**) and gene-derived DNA methylation (**FBXO28**, **PLAGL1**) at a $p \leq 0.00001$, and genes-derived SNP (**MAGI2**), ROIs (**CRBLCrus1.L**), and gene-derived DNA methylation (**FBXO28**) at a $p \leq 0.000001$, which are identified to have high interaction effects on hippocampal volume of SZ patients and healthy control.

To confirm this discovery, we used the DAVID, and gene ontology (GO) enrichment analysis to find the most relevant GO terms associated with the selected 31 genes. The selected genes are associated with a set of annotation terms. We compared 5 annotation categories, including litera-

ture, disease, gene ontology, pathways and protein interaction using DAVID (Huang, Sherman, & Lempicki, 2009). Table 7 (in the appendix) presents five annotation categories of the 31 selected genes. From this table, we observed that the selected genes have had remarkable literature review done in past studies. According to the disease annotation, the selected genes are highly associated with complex diseases including SZ, cognitive function, bipolar disorder, and others. By GO annotation, the selected genes have significant relationship to single-organism processes, response to stimuli, developmental processes and etc. From the table, we observed that the selected genes have a significant pathway to facilitate biological interpretation in a network context. Moreover, protein interaction annotations show that the selected genes have been discussed in many biomedical papers (Sanders, Duan, Levinson, & et. al., 2008; Gerhard, Wagner, Feingold, & et al., 2004; Strausberg, Feingold, Grouse, & et al., 2002).

Genes do not function alone. Rather, they interact with each other. When genes share a similar set of GO annotation terms, they are most likely to be involved in similar biological mechanisms. To confirm this, we extracted the (gene-derived SNPs)-(gene-derived DNA methylations) network using STRING (Szklarczyk et al., 2007). STRING imports protein association knowledge from databases of physical interaction and databases of curated biological pathway knowledge. In STRING, the simple interaction unit is the functional association (functional relationship between two proteins/ genes) that is most likely contributing to a common biological purpose. In this view, the color saturation of the edges represents the confidence score of a functional association. Further network analysis shows that the number of nodes, expected number of edges, number of edges, average node degree, clustering coefficient, PPI enrichment p -values are 51, 93, 300, 11.8, 0.603, and $p \leq 0 \times 10^{-16}$, respectively (Szklarczyk et al., 2007). This network has significantly more interactions than expected. This means that these genes have more interactions among themselves than what would be expected for a random set of genes of similar size drawn from the genome. Such an enrichment indicates that the proteins/genes are at least biologically connected as a group.

Lastly, we conducted standard logistic regression analysis with covariates of age, gender, and BMI on the outcome of SZ disease (SZ vs healthy control). We found that BMI is a significant covariate for the SZ vs healthy control at a $p \leq 0.0353$. Thus, BMI is one of the risk factors of SZ disease. For a BMI ≥ 25 , we considered the subject to be a high risk. Based on this risk, we divided the estimated higher order interaction effect $\hat{h}_{M^{(1)} \times M^{(2)} \times M^{(3)}}$ values into four regimes: SZ with high BMI risk, SZ with low BMI risk, healthy control with high BMI risk, and healthy control with low BMI risk. Figure 6 shows the boxplots of the estimated interaction effect within each of the four regimes for the most significant triplet (**MAGI2**, **CRBLCrus1.L**, and **FBXO28**). The

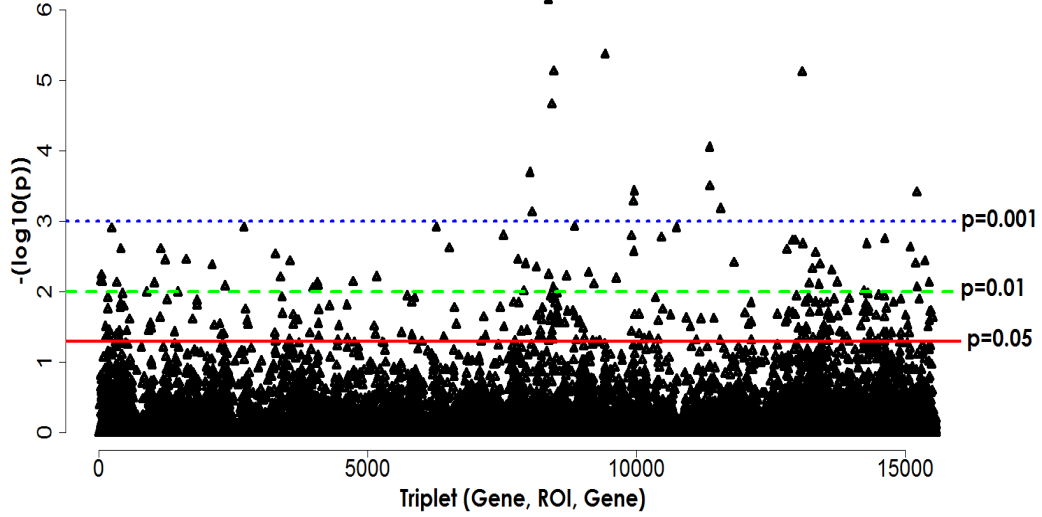


Figure 3: The plot of $-\log_{10}(p)$ with 15436 triplets.

Table 2: The selected significant genes-derived SNP, ROIs and gene-derived DNA methylation using the proposed method (KMDHOI) and SKAT. The p -values threshold was fixed to 0.001.

Genetics	Imaging	Epigenetics	σ^2	$\tau^{(1)}$	$\tau^{(2)}$	$\tau^{(3)}$	KMDHOI				OVA	HOI	SKAT HOI
							$\tau^{1 \times 2}$	$\tau^{1 \times 3}$	$\tau^{2 \times 3}$	$\tau^{1 \times 2 \times 3}$			
IL1B	CAU.R	FBXO28	0.6755	0.0038	0.0229	0.1225	1.1013	0.0000	0.1307	1.3606	0.0383	$2E-04$	0.4943
IL1B	PoCG.R	FBXO28	0.5837	0.0189	0.1827	0.1247	1.8403	0.0000	0.3469	1.0603	0.0202	$7E-04$	0.2871
MAGI2	CRBLCrus1.L	FBXO28	0.1833	0.3246	0.0000	0.2693	1.1963	2.2426	1.3683	0.0100	0.0288	$0E-06$	0.01891
MAGI2	LING.L	CRABP1	0.1813	0.4366	0.0000	0.0885	1.5370	2.6299	1.0271	0.0100	0.0470	$0E-05$	0.4030
MAGI2	IPL.R	FBXO28	0.1833	0.3778	0.0000	0.3044	0.9808	2.3888	1.2203	0.0100	0.0457	$0E-05$	0.5592
NRG1	IPL.L	PLAGL1	0.3682	0.0024	0.2162	0.1270	1.1227	2.7930	0.0000	0.2056	0.0284	$0E-05$	0.6664
PDLIM5	IPL.L	DUSP1	0.3648	0.0000	0.0804	0.2182	1.5177	1.9409	1.0276	0.0100	0.0183	$5E-04$	0.0173
PDLIM5	PoCG.R	DUSP1	0.3598	0.0000	0.2256	0.0139	0.9189	1.7853	1.2796	0.0100	0.0498	$Ee-04$	0.2761
SLC18A1	ORBsup.R	FHIT	0.4096	0.0065	0.5356	0.2276	1.3456	0.0000	1.0003	0.1323	0.0495	$1E-04$	0.0522
SLC18A1	ORBsup.R	PLAGL1	0.2869	0.0000	0.3909	0.1933	1.0186	1.3148	1.3676	0.0100	0.0373	$3E-04$	0.0149
SLC18A1	Vermis45	TFPI2	0.5571	0.0447	0.0815	0.0020	0.0000	1.0458	0.5579	0.0100	0.0354	$7E-04$	0.4234
TDRD3	CRBL8.L	FBXO28	0.5856	0.2284	0.0022	0.0702	1.1722	0.7667	0.0000	0.0100	0.0052	$0E-05$	0.0807
TDRD3	ITG.R	CRABP1	0.5291	0.2318	0.0000	0.0223	0.7052	0.6038	0.6240	0.0100	0.0033	$4E-04$	0.0359

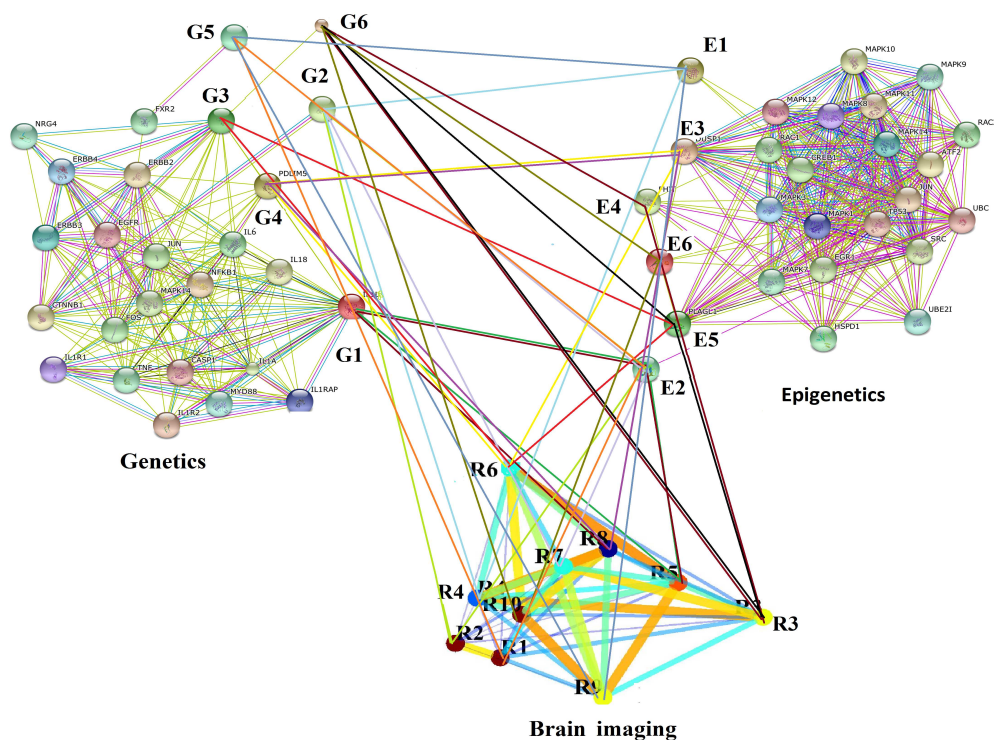


Figure 4: The network graph of features interaction of each individual view and features interactions of among others view ($p \leq 0.001$). Each node represents genes-derived SNP (**G1: IL1B**, **G2: MAGI2**, **G3: NRG1**, **G4: PDLIM5**, **G5: SLC18A1**, **G6: TDRD**), ROIs (**R1: CRBL8.L**, **R2: CRBLCrus1.L**, **R3: ORBSUP.R**, **R4: LING.L**, **R5: CAU.R**, **R6: IPL.L**, **R7: IPL.R**, **R8: PoCG.L**, **R9: ITG.R**, **R10: VER54**) and gene-derived DNA methylation (**E1: CRABP1**, **E2: FBXO28**, **E3: DUSP1**, **E4: FHIT**, **E5: PLAGL1**, **E6: TFPI2**).

Table 3: The network measurements (transitivity, degree, and global efficiency) of the selected 10 ROIs for schizophrenia candidate and healthy control groups.

ROIs	Transitivity		Degree		Global efficiency	
	Schizophrenia	Healthy	Schizophrenia	Healthy	Schizophrenia	Healthy
R1 = CRBL8.L	0.571	1.000	7	2	0.800	0.317
R2 = CRBLCrus1.L	0.600	0.333	6	3	0.750	0.400
R3 = ORBSUP.R	0.667	0.000	3	1	0.5833	0.100
R4 = LING.L	0.667	0.333	7	3	0.800	0.400
R5 = CAU.R	0.700	0.000	5	1	0.683	0.100
R6 = IPL.L	1.000	1.000	2	2	0.500	0.317
R7 = IPL.R	0.667	1.000	4	2	0.650	0.317
R8 = PoCG.L	0.667	1.000	7	2	0.800	0.3167
R9 = ITG.R	0.900	0.000	5	1	0.683	0.100
R10 = VER45	0.800	0.000	6	1	0.750	0.100

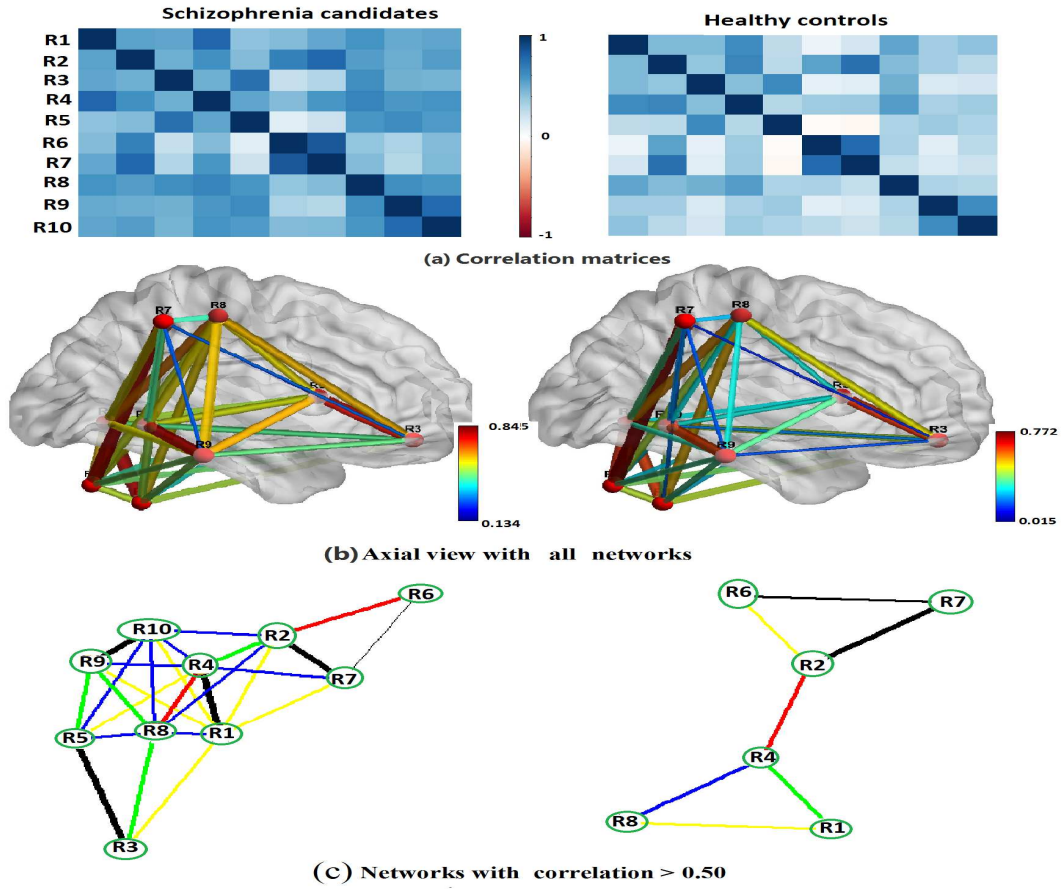


Figure 5: The visualization of selected 10 ROIs for schizophrenia candidate and healthy control groups: (a) correlation matrices, (b) axial view with all networks, (c) networks with correlation > 0.5 .

Table 4: The selected significant gene-derived SNPs, ROIs and gene-derived DNA methylations using the proposed method (KMDHOI) and SKAT at $p \leq 0.01$. The bold indicates significant at $p \leq 0.001$. Note: the name of ROI is given by the AAL template.

Genetics	IL1B	MAG12	NRG1	PDLIM5	SLC18A1	TDRD3	BDNF	CHGA	CHGB	CLINT1
	COMTD1	DAOA	DISC1	DRD2	DTNBP1	ERBB4	GABBR1	GABRB2	GRIN2B	GRM3
	HTR2A	IL10RA	MAG11	MICB	NOS1AP	NOTCH4	NR4A2	NUMBL	PLXNA2	PPP3CC
	SNAP29									
Imaging	CRBL8.L	CRBLCrus1.L	ORBSUP.R	LING.L	CAUR	IPL.L	IPL.R	PoCG.L	ITG.R	VER45
	AMYG.L	CRBL10.R	CRBL10.L	CRBL3.R	CRBL3.R	CRBL45.L	CRBL6.L	CRBL8.R	CRBLCrus2.R	CRBLCrus2.L
	DCG.R	DCG.L	PCG.R	ORBsup.L	ORBmid.R	LING.R	ROL.R	SMA.R	TPOsup.R	TPOsup.L
	STG.L	ITG.L	Vermis10	Vermis3	MTG.R					
Epigenetic	CRABP1	FBXO28	DUSP1	FHIT	PLAGL1	TFPI2	CCND2	CDKN1A	EDNRB	ESR1
	EYA4	FEN1	GPSN2	HOXA9	HOXB4	PTGS2	RB1	SRF	WDR37	ZNF512

small variation indicates a higher risk of the interaction effect (hippocampal volume). This figure shows that the SZ and BMI risks largely dominate the interaction effect (i.e., higher SZ and BMI risk associated with higher risk of interaction) and vice versa.

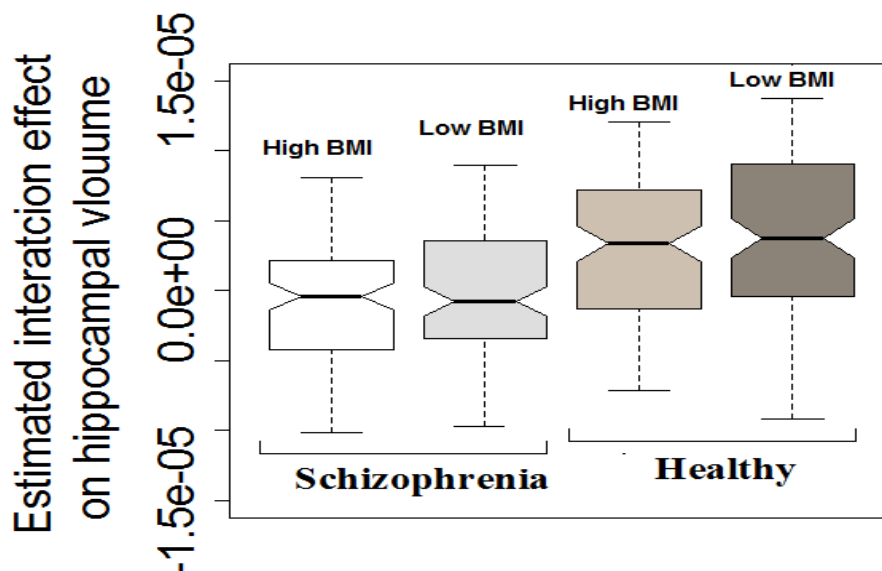


Figure 6: Boxplot of significant interaction effects in different regimes (SZ and high BMI risk, SZ and low BMI risk, healthy control and high BMI risk, healthy control and low BMI risk) for the most significant triplet (**MAGI2**, **CRBLCrus1.L**, **FBXO28**).

6 Discussion and future research

In this paper, we have proposed a semiparametric kernel method for higher order interactions between multiple data sets. Compared to the traditional PCA multiple regression and SKAT methods, the proposed method shows a more flexible and biological plausible way to model higher order epistasis among the genetic, imaging, and epigenetic data. While kernel based methods on multi-view data naturally produce more powerful and reproducible results, and are biologically more meaningful, the interpretation of model parameters is often challenging. Incorporating the gene and pathway analysis of biological information would facilitate additional improvements of model interpretation.

The performance of the proposed method was evaluated on both simulated and real MCIC data. The extensive simulation studies show evidence of the power gain of the proposed method relative to the alternative methods and suggest that the proposed methods perform remarkably better than the dimension reduction multiple regression and SKAT methods.

The utility of the proposed method is further demonstrated with the application to imaging ge-

netics study of SZ. According to the p -values, the proposed method is able to rank the triplets (gene-derived SNPs)-ROI-(gene-derived DNA methylations) and subset of triplets can be selected which are highly related to SZ disease. At a $p \leq 0.01$ the proposed method extract the unique 31 genes-derived SNP, 35 ROIs and 20 gene-derived DNA methylation from 72 triplets, which are identified to have significant impact on hippocampal volume of SZ patients. By conducting gene ontology, pathway analysis, and several network measures including visualizations, we find evidence that the selected (gene-derived SNPs)- ROI-(gene-derived DNA methylations) have a significant influence on the manifestation of SZ disease. The identified triplets suggest that these statistical and biologically significant triplets may an important role in SZ related neurodegenerations. Our findings have indicated that genetic elements interplay with brain regions and epigenetic factors.

While we illustrated the proposed model using a quantitative hippocampal volume derived from structural MRI image phenotype, the utility of this model is that it can be applied to any phenotypes to detect higher order interactions in genetics, imaging, and epigenetic features, to include environmental covariates. The proposed model can also be extended to qualitative phenotypes for potentially widely applicable case-control studies (e.g., generalized kernel logistic regression).

It must be repeated that choosing a suitable kernel is indispensable. Kernel parameters may strongly influence the result desired for its application. Although the linear kernel does not have any free parameters, the linear kernel has certain limitations. Using the polynomial kernel makes it possible to detect higher order correlations. Polynomial kernels only map data into a finite dimensional space. In addition, both linear and polynomial kernels are unbounded. Many radial basis function kernels, such as the Gaussian kernel, map input data into an infinite dimensional space. The Gaussian kernel has a free parameter (bandwidth) but follows a number of properties (e.g., boundedness, consistency, universality, and robustness).

In this study, while we applied the median of the pairwise distance as a bandwidth for the Gaussian kernel, future studies might also compare the higher order interaction effects using a number of different kernels with different parameters, which may have broad implications to the detection of higher order interactions between disease phenotypes as described in the methods of this paper.

Acknowledgments

The authors wish to thank the NIH (R01 GM109068, R01 MH104680, ROI MH107354) and NSF EPSCoR program (1539067) for support.

References

- Aberg, K. A., McClay, J. L., Nerella, S., & et al., S. C. (2014). Methylome-wide association study of schizophrenia identifying blood biomarker signatures of environmental insults. *JAMA Psychiatry*, *71*(3), 255-264.
- Alam, M. A. (2014). Kernel choice for unsupervised kernel methods. Japan: PhD. Dissertation, The Graduate University for Advanced Studies.
- Alam, M. A., Calhoun, V., & Wang, Y. P. (2016). Influence function of multiple kernel canonical analysis to identify outliers in imaging genetics data. *Proceedings of 7th ACM Conference on Bioinformatics, Computational Biology, and Health Informatics (ACM BCB)*, Seattle, WA, USA, 210-2198.
- Alam, M. A., & Fukumizu, K. (2014). Hyperparameter selection in kernel principal component analysis. *Journal of Computer Science*, *10*(7), 1139–1150.
- Alam, M. A., & Fukumizu, K. (2015). Higher-order regularized kernel canonical correlation analysis. *International Journal of Pattern Recognition and Artificial Intelligence*, *29*(4), 1551005(1-24).
- Alam, M. A., Komori, O., Calhoun, V., & Wang, Y. P. (2016). Robust kernel canonical correlation analysis to detect gene-gene interaction for imaging genetics data. *Proceedings of 7th ACM Conference on Bioinformatics, Computational Biology, and Health Informatics (ACM BCB)*, Seattle, WA, USA, 279-288.
- Andreasen, N. C. (1984). Scale for the assessment of positive symptoms (saps). Iowa City, University of Iowa: Springer.
- Aronszajn, N. (1950). Theory of reproducing kernels. *Transactions of the American Mathematical Society*, *68*, 337-404.
- Bis, J. C., DeCarli, C., & et al., A. S. (2012). Common variants at 12q14 and 12q24 are associated with hippocampal volume. *Nature Genetics*, *44*(5), 545-551.
- B. K. Sriperumbudur, A. G. G. R. G. L., K. Fukumizu, & Schölkopf, B. (2009). Kernel choice and classifiability for rkhs embeddings of probability distributions. *Advances in Neural Information Processing Systems*, *21*, 1750-1758.
- Bly, M. (2005). Mutation in the vesicular monoamine gene, *slc18a1*, associated with schizophrenia. *Schizophrenia Research*, *78*, 337-338.
- Calhoun, V. D., & Sui, J. (2016). Multimodal fusion of brain imaging data: A key to finding the missing link(s) in complex mental illness. *Biol Psychiatry Cogn Neurosci Neuroimaging*, *1*,

230-244.

- Camps-Valls, G., Rojo-Alvarez, J. L., & Martinez-Romon, M. (2007). Kernel methods in bioengineering, signal and image. London: Idea Group publishing.
- Chang, B., Kruger, U., Kustra, R., & Zhang, J. (2013). Canonical correlation analysis based on hilbert-schmidt independence criterion and centered kernel target alignment. *Proceedings of the 30th International Conference on Machine Learning, Atlanta, Georgia, USA*.
- Chekouo, T., Stingo, F. C., Guindani, M., & Do, K. A. (2016). A bayesian predictive model for imaging genetics with application to schizophrenia. *The Annals of Applied Statistics*, 10(3), 1547-1571.
- Chen, J., Calhoun, V. D., Pearlson, G. D., Ehrlich, S., Turner, J. A., Ho, B. C., . . . Liu, J. (2012). Multifaceted genomic risk for brain function in schizophrenia. *NeuroImage*, 61, 866-875.
- Chen, Z., Liu, M., Gross, D. W., & Beaulieu, C. (2013). Graph theoretical analysis of developmental patterns of the white matter network. *Frontiers in Human Neuroscience*, 7, 199-211.
- Ge, T., Nichols, T. E., Ghosh, D., Mormino, E. C., J. W. Smoller, a. M. R. S., & the Alzheimer's Disease Neuroimaging Initiative. (2015). A kernel machine method for detecting effects of interaction between multidimensional variable sets: An imaging genetics application. *NeuroImage*, 109, 505-514.
- Gerhard, D. S., Wagner, L., Feingold, E. A., & et al. (2004). The status, quality, and expansion of the nih full-length cDNA project: the mammalian gene collection (mgc). *The American Journal of Psychiatry*, 14(10B), 2121-7.
- Gollub, R. L., Shoemaker, J. M., King, M. D., White, T., Ehrlich, S., Sponheim, S. R., . . . Andreasen, N. C. (2013). The mcic collection: a shared repository of multi-modal, multi-site brain image data from a clinical investigation of schizophrenia. *Front Genet*, 11, 367-38.
- Gretton, A., Fukumizu, K., Teo, C. H., Song, L., Schölkopf, B., & Smola, A. (2008). A kernel statistical test of independence. *In Advances in Neural Information Processing Systems*, 20, 585-592.
- Harrison, P. J., & Law, A. J. (2006). Neuregulin 1 and schizophrenia: Genetics, gene expression, and neurobiology. *BIOL PSYCHIATRY*, 60, 132-140.
- Harville, D. A. (1974). Bayesian inference for variance components using only error contrasts. *Biometrika*, 61(2), 383-385.
- Hieke, S., Binder, H., Nieters, A., & Schumacher, M. (2014). Convergence analysis of kernel canonical correlation analysis: theory and practice. *Computational Statistics*, 29(1-2), 51-63.

- Hofmann, T., Schölkopf, B., & Smola, J. A. (2008). Kernel methods in machine learning. *The Annals of Statistics*, 36, 1171-1220.
- Huang, D., Sherman, B. R., & Lempicki, R. A. (2009). Systematic and integrative analysis of large gene lists using david bioinformatics resources. *Nature Protocols*, 4(1), 44-57.
- I. Ionita-Laza, V. M. J. B. X. L. X. ., S. Lee. (2013). Sequence kernel association tests for the combined effect of rare and common variants. *American Journal of Human Genetics*, 92, 841-853.
- Jahanshad, N., Hibar, D. P., Ryles, A., Toga, A. W., McMahon, K. L., de Zubicaray, G. I., ... Thompson, P. M. (2012). Discovery of genes that affect human brain connectivity: A genome-wide analysis of the connectome. *In Proceeding IEEE Int Symp Biomed Imaging*, 542-545.
- Jahanshad, N., & X. Hua, e. a. (2013). Genome-wide scan of healthy human connectome discovers spon1 gene variant influencing dementia severity. *In Proceedings of the National Academy of Sciences*, 110(12), 4768-73.
- Kimeldorf, G., & Wahhba, G. (1971). Some results on tchebycheffian spline functions. *Journal of mathematical analysis and applications*, 33(1), 82-95.
- Kircher, T., & Renate, T. (2005). Functional brain imaging of symptoms and cognition in schizophrenia. *Progress in Brain Research*, 150, 299308.
- Koide, T., Banno, M., Aleksic, B., & et al. (2013). Common variants in magi2 gene are associated with increased risk for cognitive impairment in schizophrenic patients. *PLoS ONE*, 7(9), e36836.
- Kung, S. Y. (2014). Kernel methods and machine learning. New York: Cambridge University Press.
- Laid, N., Lange, N., & Stram, D. (1987). Maximum likelihood computations with repeated measures: Application of the em algorithm. *Journal of the American Statistical Association*, 82(397), 97-105.
- L. C. Kwee, X. L. D. G. M. P. E., D. Liu. (2008). A powerful and flexible multilocus association test for quantitative traits. *Annals of Human Genetics*, 82(2), 386-397.
- Lencz, T., Morgan, T. V., Athanasiou, M., Dain, B., Reed, C. R., Kane, J. M., ... Malhotra, A. K. (2007). Converging evidence for a pseudoautosomal cytokine receptor gene locus in schizophrenia. *Molecular Psychiatry*, 12, 572-580.
- Li, J., Huang, D., Guo, M., Liu, X., Wang, C., Teng, Z., ... Wang, L. (2015). A gene-based information gain method for detecting genegene interactions in casecontrol studies. *European*

- Journal of Human Genetics*, 23, 1566-1572.
- Li, S., & Cui, Y. (2012). Gene-centric gene-gene interaction: a model-based kernel machine method. *The Annals of Applied Statistics*, 6(3), 1134-1161.
- Lin, D., Callhoun, V. D., & Wang, Y. P. (2014). Correspondence between fmri and snp data by group sparse canonical correlation analysis. *Medical Image Analysis*, 18, 891 - 902.
- Lindstrom, M. J., & Bates, M. D. (1988). Newton-raphson and em algorithms for linear mixed-effects models for repeated-measures data. *Journal of the American Statistical Association*, 83(404), 1014-1022.
- Liu, D., Lin, X., & Ghosh, D. (2007). Semiparametric regression of multidimensional genetics pathway data: least squares kernel machines and linear mixed model,. *Biometrics*, 63(4), 1079-1088.
- Liu, J., Chen, J., Ehrlich, S., Walton, E., T. White, N. P. B., Bustillo, J., ... Calhoun, V. D. (2014). Methylation patterns in whole blood correlate with symptoms in schizophrenia patients. *Schizophrenia Bulletin*, 40(4), 769-776.
- Liu, M., Min, R., Y. Gao, D. Z., & Shen, D. (2016). Multitemplate-based multiview learning for alzheimers disease diagnosis machine learning and medical imaging. *Machine Learning and Medical Imaging*, 259-297.
- Montano, C., Tauband, M. A., Jaffe, A., Briem, E., & et al. (2016). Association of dna methylation differences with schizophrenia in an epigenome-wide association study. *JAMA Psychiatry*, 73(5), 506-514.
- Moselhy, H., Eapenb, V., Akawi, N. A., Younis, A., & et. al. (2015). Secondary association of pdlim5 with paranoid schizophrenia in emirati patients. *Meta Gene*, 5, 135-139.
- Parkhomenko, E., Tritchler, D., & Beyene, J. (2009). Sparse canonical correlation analysis with application to genomic data integration. *Statistical Applications in Genetics and Molecular Biology*, 8(1), 1-34.
- Pearlson, G. D., Liu, J., & Calhoun, V. D. (2015). An introductory review of parallel independent component analysis (p-ica) and a guide to applying p-ica to genetic data and imaging phenotypes to identify disease-associated biological pathways and systems in common complex disorders. *Front Genet*, 6, 276.
- Peng, Q. N., Zhao, J., & Xue, F. (2010). A gene-based method for detecting genegene co-association in a casecontrol association study. *European Journal of Human Genetics*, 18, 582-587.
- Potkin, S. G., T. G. M. Van, E., Ling, S., Macciardi, F., & Xie, X. (2015). Unanticipated genes and mechanisms in serious mental illness: Gwas based imaging genetics strategies. In (Vol. 209).

- London: Oxford University Press.
- Richfield, O., Alam, M. A., Calhoun, V., & Wang, Y. P. (2017). Learning schizophrenia imaging genetics data via multiple kernel canonical correlation analysis. *Proceedings - 2016 IEEE International Conference on Bioinformatics and Biomedicine, BIBM 2016, Shenzhen, China*, 5, 507-5011.
- Sanders, A. R., Duan, J., Levinson, D. F., & et. al. (2008). No significant association of 14 candidate genes with schizophrenia in a large european ancestry sample: implications for psychiatric genetics. *The American Journal of Psychiatry*, 165(10), 1359-1368.
- Satterthwaite, F. E. (1946). An approximate distribution of estimates of variance components. *Biometrics Bulletin*, 2(6), 110-114.
- Schölkopf, B., & Smola, A. J. (2002). *Learning with kernels*. Cambridge MA: MIT Press.
- Schölkopf, B., Smola, A. J., & Müller, K.-R. (1998). Nonlinear component analysis as a kernel eigenvalue problem. *Neural Computation*, 10, 1299-1319.
- Shibuya, M., Watanabe, Y., Nunokawa, A., Egawa, J., Kaneko, N., Igeta, H., & Someya, T. (2013). Interleukin 1 beta gene and risk of schizophrenia: detailed casecontrol and family-based studies and an updated meta-analysis. *Human Psychopharmacology*, 29, 31-37.
- Siawa, G. E.-L., Liuc, I.-F., Linc, P. Y., Beend, M. D., & Hsiehc, T. (2016). Dna and rna topoisomerase activities of top3 are promoted by mediator protein tudor domain-containing protein 3. *Proc Natl Acad Sci USA*, 113, 5544-5551.
- Sluis, S. V. D., Dolan, C. V., Li, J., Song, Y., Sham, P., Posthumal, D., & Li, M. (2015). Mgas: a powerful tool for multivariate gene-based genome-wide association analysis. *Bioinformatics*, 31, 1007-1015.
- Song, L., Smola, A., Gretton, A., Bedo, J., & Borgwardt, K. (2012). Feature selection via dependence maximization. *Journal of Machine Learning Research*, 13, 1393-1434.
- Strausberg, R. L., Feingold, E. A., Grouse, L. H., & et al. (2002). Generation and initial analysis of more than 15,000 full-length human and mouse cdna sequences. *Proceedings of the National Academy of Sciences, USA*, 99(26), 16899-903.
- Suk, H., Wee, C., Lee, S., & Shen, D. (2016). State-spacemodel with deep learning for functional dynamics estimation in resting-state fmri. *NeuroImage*, 129, 292-307.
- S. Yu, B. D. M., L-C. Tranchevent, & Moreau, Y. (2011). Kernel-based data fusion for machine learning. Verlag Berlin Heidelberg: Springer.
- Szklarczyk, D., Franceschini, A., Wyder, S., Forslund, K., Heller, D., Huerta-Cepas, J., . . . von Mering, C. (2007). STRING v10: Proteinprotein interaction networks, integrated over the

- tree of life. *Nucleic Acids Research*, 43, 531–543.
- Van, S. O., & Kapur, S. (2009). Schizophrenia. *Lancet*, 374 (9690), 635645.
- Wan, X., Yang, C., Yang, Q., Xue, H., Fan, X., Tang, N. L., & Yu, W. (2010). Boost: A fast approach to detecting gene-gene interactions in genome-wide case-control studies. *The American Journal of Human Genetics*, 87, 325-340.
- Wen, H., Liu, Y., Rekik, I., Wang, S., Chen, Z., Zhang, J., . . . He, H. (2017). Multi-modal multiple kernel learning for accurate identification of tourette syndrome children. *Pattern Recognition*, 63, 601-611.
- Wockner, L. F., Noble, E. P., Lawford, B. R., Young, R. M., Morris, C. P., Whitehall, V. L. J., & Voisey, J. (2014). Genome-wide dna methylation analysis of human brain tissue from schizophrenia patients. *Transl Psychiatry*, 4 (e339), 1-8.
- Wu, K., Taki, Y., Sato, K., Oi, H., Kawashima, R., & Fukuda, H. (2013). A longitudinal study of structural brain network changes with normal aging. *Frontiers in Human Neuroscience*, 7, 225-236.
- Wu, M. C., Lee, S., Cai, T., Li, Y., Boehnke, M., & Lin, X. (2011). Rare variant association testing for sequencing data using the sequence kernel association test (SKAT). *American Journal of Human Genetics*, 89, 82-93.
- Xu, C., Tao, D., & Xu, C. (2013). A survey of multi-view machine learning. *Neural Computation and Applications*, 23(7-8), 2031-2038.
- Yan, C., & Zang, Y. (2010). DPARSF: a MATLAB toolbox for pipeline data analysis of resting-state fMRI. *Frontiers in Systems Neuroscience*, 4 (13), 1-7.
- Yuan, Z., Gao, Q., He, Y., Zhang, X., Li, F., Zhao, J., & Xue, F. (2012). Detection for gene-gene co-association via kernel canonical correlation analysis. *BMC Genetic*, 13:83.
- Zhao, F., Qiao, L., F. Shi, P. T. Y., & Shen, D. (2016). Feature fusion via hierarchical supervised local cca for diagnosis of autism spectrum disorder. *Brain Imaging and Behavior*, 1-11.
- Zheng, S., Cai, X., Ding, C. H., Nie, F., & Hung, H. (2015). A closed form solution to multi-view low-rank regression. *In Proceedings of the Twenty-Ninth AAAI Conference on Artificial Intelligence, (AAAI-15)*, 1973-1979.

Appendix

In the following sections, we present the details of the proposed method, Satterthwaite approximation to the score test, in addition we present supplementary tables and figures on our methods to

their application to imaging genetics and epigenetics.

A Estimation of the linear mixed effect model using ReML

As discussed in the literature, we can estimate the variance components using the restricted maximum likelihood (ReML) approach (Harville, 1974; Lindstrom & Bates, 1988). The restricted log-likelihood function of Eq. (13) is written as:

$$\ell_R(\boldsymbol{\theta}) = -\frac{1}{2}\ln(|\Theta(\boldsymbol{\theta})|) - \frac{1}{2}\ln(|\mathbf{X}^T \Theta^{-1}(\boldsymbol{\theta}) \mathbf{X}|) - \frac{1}{2}(\mathbf{y} - \mathbf{X}\hat{\boldsymbol{\beta}})^T \Theta^{-1}(\boldsymbol{\theta})(\mathbf{y} - \mathbf{X}\hat{\boldsymbol{\beta}}) \quad (\text{A.1})$$

where $\hat{\boldsymbol{\beta}}$ is the BLUP of the regression coefficients $\boldsymbol{\beta}$ $\Theta(\boldsymbol{\theta}) = \sigma^2 \mathbf{I} + \tau^{(1)} \mathbf{K}^{(1)} + \tau^{(2)} \mathbf{K}^{(2)} + \tau^{(3)} \mathbf{K}^{(3)} + \tau^{(1 \times 2)} \mathbf{K}^{(1 \times 2)} + \tau^{(1 \times 3)} \mathbf{K}^{(1 \times 3)} + \tau^{(2 \times 3)} \mathbf{K}^{(2 \times 3)} + \tau^{(1 \times 2 \times 3)} \mathbf{K}^{(1 \times 2 \times 3)}$, where $\boldsymbol{\theta} = (\sigma^2, \tau^{(1)}, \tau^{(2)}, \tau^{(3)}, \tau^{1 \times 2}, \tau^{2 \times 3}, \tau^{1 \times 2 \times 3})$ are the variance components. To estimate the variance components, we need to perform the partial derivative of Eq. (A.1) with respect to each variance component:

$$\begin{aligned} \frac{\partial \ell_R}{\partial \theta_i} &= -\frac{1}{2} \text{tr}(\mathbf{W} \mathbf{G}_i) + \frac{1}{2} (\mathbf{y} - \mathbf{X}\hat{\boldsymbol{\beta}})^T \Theta^{-1}(\boldsymbol{\theta}) \mathbf{G}_i \Theta^{-1}(\boldsymbol{\theta}) \mathbf{1}^T (\mathbf{y} - \mathbf{X}\hat{\boldsymbol{\beta}}) \\ &= -\frac{1}{2} \text{tr}(\mathbf{W} \mathbf{G}_i) + \frac{1}{2} \mathbf{y}^T \mathbf{W} \mathbf{G}_i \mathbf{W} \mathbf{y} = 0 \end{aligned} \quad (\text{A.2})$$

where $\mathbf{G}_i = \frac{\partial \Theta}{\partial \theta_i}$ and $\mathbf{W} = \Theta^{-1} - \Theta^{-1} \mathbf{X} (\mathbf{X}^T \Theta^{-1} \mathbf{X})^{-1} \mathbf{X}^T \Theta^{-1}$. We also have $\frac{\partial \Theta}{\partial \sigma^2} = \mathbf{I}$, $\frac{\partial \Theta}{\partial \tau^{(1)}} = \mathbf{K}^{(1)}$, $\frac{\partial \Theta}{\partial \tau^{(2)}} = \mathbf{K}^{(2)}$, $\frac{\partial \Theta}{\partial \tau^{(3)}} = \mathbf{K}^{(3)}$, $\frac{\partial \Theta}{\partial \tau^{(1 \times 2)}} = \mathbf{K}^{(1 \times 2)}$, $\frac{\partial \Theta}{\partial \tau^{(1 \times 3)}} = \mathbf{K}^{(1 \times 3)}$, $\frac{\partial \Theta}{\partial \tau^{(1 \times 2 \times 3)}} = \mathbf{K}^{(1 \times 2 \times 3)}$. The (i, j) -th element of the observed and expected information matrices are

$$\left[\frac{\partial^2 \ell_R}{\partial \theta_i \partial \theta_j} \right]_{ij} = -\frac{1}{2} \text{tr}(\mathbf{W} \mathbf{G}_i \mathbf{W} \mathbf{G}_j) + \mathbf{y}^T \mathbf{W} \mathbf{G}_i \mathbf{W} \mathbf{G}_j \mathbf{W} \mathbf{y},$$

$$\mathbf{E} \left[\frac{\partial^2 \ell_R}{\partial \theta_i \partial \theta_j} \right]_{ij} = -\frac{1}{2} \text{tr}(\mathbf{W} \mathbf{G}_i \mathbf{W} \mathbf{G}_j) = \mathcal{I}(\boldsymbol{\theta}),$$

respectively. Using Fisher's scoring algorithm (Newton-Raphson method to solve maximum likelihood equations numerically), given an initial value of unknown parameters at the h -th iteration $\boldsymbol{\theta}_{(k+1)}$, the parameters are updated as

$$\boldsymbol{\theta}_{(k+1)} = \boldsymbol{\theta}_{(k)} + [\mathcal{I}(\boldsymbol{\theta}_{(h)}^{-1})] \left[\frac{\partial \ell_R}{\partial \boldsymbol{\theta}} \right]_{\boldsymbol{\theta}_{(k)}}.$$

In expectation maximization (EM) algorithm, we used a set of initial points (0, 0.00001, 0.0001, 0.001, 0.01, 0.1, 1) of the variance components for the optimization algorithm and chose the best

one (maximized ReML) to avoid the local minim (Laid, Lange, & Stram, 1987). For the σ^2 , we fixed initial values to $\text{Var}(\mathbf{y})$. After EM update, we then conducted the Fisher's scoring algorithm for the left iterations until the difference between successive log ReML values ($|\ell_{R(h+1)} - \ell_{R(h)}|$) was smaller than 10^{-05} . In most cases the ReML algorithm converged in less than 50 iterations and in some cases it converged very quickly with 10 iterations, taking only a few seconds with an R-program.

B Satterthwaite approximation to the score test

The restricted score function under the null hypothesis $H_0 : \tau^{(1)} = \tau^{(2)} = \tau^{(3)} = \tau^{(1 \times 2)} = \tau^{(1 \times 3)} = \tau^{(2 \times 3)} = \tau^{(1 \times 2 \times 3)} = 0$ is given by:

$$\frac{\partial \ell_R}{\partial \theta_i} \Big|_{\tau=0} = -\frac{1}{2\sigma^2} \text{tr}(\mathbf{W}_0 \mathbf{G}_i) + \frac{1}{2\sigma^4} (\mathbf{y} - \mathbf{X}\hat{\boldsymbol{\beta}})^\top \boldsymbol{\Theta}^{-1} \mathbf{G}_i (\mathbf{y} - \mathbf{X}\hat{\boldsymbol{\beta}}) \quad (\text{B.1})$$

where $\mathbf{W}_0 = \mathbf{I} - \mathbf{I}(\mathbf{I}^\top \mathbf{I})^{-1} \mathbf{I}^\top$ and $\boldsymbol{\tau} = \tau^{(1)} = \tau^{(2)} = \tau^{(3)} = \tau^{(1 \times 2)} = \tau^{(1 \times 3)} = \tau^{(2 \times 3)}$. Since the MLE is \sqrt{n} consistent, the asymptotic distribution of $S(\hat{\sigma}_0^2)$ can still be approximated by the scaled chi-square distribution. By considering the true value of σ^2 under null hypothesis as σ_0^2 , the mean and variance of the test statistic $S(\hat{\sigma}_0^2)$ are:

$$E[S(\sigma_0^2)] = \frac{1}{2} \text{tr}(\mathbf{W}_0 \mathbf{K}) = E[\gamma \chi_\nu^2] = \gamma \nu, \text{ and}$$

$$\text{Var}[S(\sigma_0^2)] = \frac{1}{2} \text{tr}(\mathbf{W}_0 \mathbf{K} \mathbf{W}_0 \mathbf{K}) = \text{Var}[\gamma \chi_\nu^2] = 2\gamma^2 \nu$$

where $\mathbf{K} = \mathbf{K}^{(1)} + \mathbf{K}^{(2)} + \mathbf{K}^{(3)} + \mathbf{K}^{(1 \times 2)} + \mathbf{K}^{(1 \times 3)} + \mathbf{K}^{(2 \times 3)} + \mathbf{K}^{(1 \times 2 \times 3)}$ and $\hat{\boldsymbol{\beta}}$. To account for this substitution, we need to estimate γ and ν by replacing the $\text{Var}[S(\hat{\sigma}_0^2)]$ based on the efficient information. The elements of the Fisher information matrix $\boldsymbol{\tau}$ are written as:

$$I_{\boldsymbol{\tau}\boldsymbol{\tau}} = \begin{bmatrix} \text{tr}(\mathbf{A}^{(1)} \mathbf{A}^{(1)}) & \text{tr}(\mathbf{A}^{(1)} \mathbf{A}^{(2)}) & \text{tr}(\mathbf{A}^{(1)} \mathbf{A}^{(3)}) & \text{tr}(\mathbf{A}^{(1)} \mathbf{A}^{(1 \times 2)}) & \text{tr}(\mathbf{A}^{(1)} \mathbf{A}^{(1 \times 3)}) & \text{tr}(\mathbf{A}^{(1)} \mathbf{A}^{(2 \times 3)}) & \text{tr}(\mathbf{A}^{(1)} \mathbf{A}^{(1 \times 2 \times 3)}) \\ \text{tr}(\mathbf{A}^{(2)} \mathbf{A}^{(1)}) & \text{tr}(\mathbf{A}^{(2)} \mathbf{A}^{(2)}) & \text{tr}(\mathbf{A}^{(2)} \mathbf{A}^{(3)}) & \text{tr}(\mathbf{A}^{(2)} \mathbf{A}^{(1 \times 2)}) & \text{tr}(\mathbf{A}^{(2)} \mathbf{A}^{(1 \times 3)}) & \text{tr}(\mathbf{A}^{(2)} \mathbf{A}^{(2 \times 3)}) & \text{tr}(\mathbf{A}^{(2)} \mathbf{A}^{(1 \times 2 \times 3)}) \\ \text{tr}(\mathbf{A}^{(3)} \mathbf{A}^{(1)}) & \text{tr}(\mathbf{A}^{(3)} \mathbf{A}^{(2)}) & \text{tr}(\mathbf{A}^{(3)} \mathbf{A}^{(3)}) & \text{tr}(\mathbf{A}^{(3)} \mathbf{A}^{(1 \times 2)}) & \text{tr}(\mathbf{A}^{(3)} \mathbf{A}^{(1 \times 3)}) & \text{tr}(\mathbf{A}^{(3)} \mathbf{A}^{(2 \times 3)}) & \text{tr}(\mathbf{A}^{(3)} \mathbf{A}^{(1 \times 2 \times 3)}) \\ \text{tr}(\mathbf{A}^{(1 \times 2)} \mathbf{A}^{(1)}) & \text{tr}(\mathbf{A}^{(1 \times 2)} \mathbf{A}^{(2)}) & \text{tr}(\mathbf{A}^{(1 \times 2)} \mathbf{A}^{(3)}) & \text{tr}(\mathbf{A}^{(1 \times 2)} \mathbf{A}^{(1 \times 2)}) & \text{tr}(\mathbf{A}^{(1 \times 2)} \mathbf{A}^{(1 \times 3)}) & \text{tr}(\mathbf{A}^{(1 \times 2)} \mathbf{A}^{(2 \times 3)}) & \text{tr}(\mathbf{A}^{(1 \times 2)} \mathbf{A}^{(1 \times 2 \times 3)}) \\ \text{tr}(\mathbf{A}^{(1 \times 3)} \mathbf{A}^{(1)}) & \text{tr}(\mathbf{A}^{(1 \times 3)} \mathbf{A}^{(2)}) & \text{tr}(\mathbf{A}^{(1 \times 3)} \mathbf{A}^{(3)}) & \text{tr}(\mathbf{A}^{(1 \times 3)} \mathbf{A}^{(1 \times 2)}) & \text{tr}(\mathbf{A}^{(1 \times 3)} \mathbf{A}^{(1 \times 3)}) & \text{tr}(\mathbf{A}^{(1 \times 3)} \mathbf{A}^{(2 \times 3)}) & \text{tr}(\mathbf{A}^{(1 \times 3)} \mathbf{A}^{(1 \times 2 \times 3)}) \\ \text{tr}(\mathbf{A}^{(2 \times 3)} \mathbf{A}^{(1)}) & \text{tr}(\mathbf{A}^{(2 \times 3)} \mathbf{A}^{(2)}) & \text{tr}(\mathbf{A}^{(2 \times 3)} \mathbf{A}^{(3)}) & \text{tr}(\mathbf{A}^{(2 \times 3)} \mathbf{A}^{(1 \times 2)}) & \text{tr}(\mathbf{A}^{(2 \times 3)} \mathbf{A}^{(1 \times 3)}) & \text{tr}(\mathbf{A}^{(2 \times 3)} \mathbf{A}^{(2 \times 3)}) & \text{tr}(\mathbf{A}^{(2 \times 3)} \mathbf{A}^{(1 \times 2 \times 3)}) \\ \text{tr}(\mathbf{A}^{(1 \times 2 \times 3)} \mathbf{A}^{(1)}) & \text{tr}(\mathbf{A}^{(1 \times 2 \times 3)} \mathbf{A}^{(2)}) & \text{tr}(\mathbf{A}^{(1 \times 2 \times 3)} \mathbf{A}^{(3)}) & \text{tr}(\mathbf{A}^{(1 \times 2 \times 3)} \mathbf{A}^{(1 \times 2)}) & \text{tr}(\mathbf{A}^{(1 \times 2 \times 3)} \mathbf{A}^{(1 \times 3)}) & \text{tr}(\mathbf{A}^{(1 \times 2 \times 3)} \mathbf{A}^{(2 \times 3)}) & \text{tr}(\mathbf{A}^{(1 \times 2 \times 3)} \mathbf{A}^{(1 \times 2 \times 3)}) \end{bmatrix},$$

$$I_{\tau\sigma^2} = \frac{1}{2} [\text{tr}(\mathbf{A}^{(1)}) \quad \text{tr}(\mathbf{A}^{(2)}) \quad \text{tr}(\mathbf{A}^{(3)}) \quad \text{tr}(\mathbf{A}^{(1 \times 2)}) \quad \text{tr}(\mathbf{A}^{(1 \times 3)}) \quad \text{tr}(\mathbf{A}^{(2 \times 3)}) \quad \text{tr}(\mathbf{A}^{(1 \times 2 \times 3)})],$$

and $\mathcal{I}_{\sigma^2\sigma^2} = \frac{1}{2}\text{tr}(\mathbf{W}_0\mathbf{W}_0)$, where $\mathbf{A}^{(1)} = \mathbf{W}_0\mathbf{K}^{(1)}$, $\mathbf{A}^{(2)} = \mathbf{W}_0\mathbf{K}^{(2)}$, $\mathbf{A}^{(3)} = \mathbf{W}_0\mathbf{K}^{(3)}$, $\mathbf{A}^{(1 \times 2)} = \mathbf{W}_0\mathbf{K}^{(1 \times 2)}$, $\mathbf{A}^{(1 \times 3)} = \mathbf{W}_0\mathbf{K}^{(1 \times 3)}$, $\mathbf{A}^{(2 \times 3)} = \mathbf{W}_0\mathbf{K}^{(2 \times 3)}$, $\mathbf{A}^{(1 \times 2 \times 3)} = \mathbf{W}_0\mathbf{K}^{(1 \times 2 \times 3)}$. Using these information matrices, we have the efficient information $\tilde{\mathcal{I}}_{\tau\tau} = \mathcal{I}_{\tau,\tau} - \mathcal{I}_{\tau\sigma^2}^T \mathcal{I}_{\sigma^2\sigma^2}^{-1} \mathcal{I}_{\tau\sigma^2}$ and $\text{Var}[S(\hat{\sigma}_0^2)] = \text{SUM}[\tilde{\mathcal{I}}_{\tau\tau}]$, where the operator "SUM" indicates the sum of all the element in the matrix. By considering the adjusted parameters $\hat{\gamma} = \frac{\text{Var}[S(\hat{\sigma}_0^2)]}{2\text{E}[S(\hat{\sigma}_0^2)]}$ and $\hat{\nu} = \frac{2\text{E}[S(\hat{\sigma}_0^2)]^2}{\text{Var}[S(\hat{\sigma}_0^2)]}$, the p -value of an experimental score statistic $S(\hat{\sigma}_0^2)$ is obtained using the scaled chi-square distribution $\hat{\gamma}\chi_{\hat{\nu}}^2$.

The score test statistic $S_I(\tilde{\tau}_I)$ defined in Eq. (16) for the higher order interaction effect that testing the null hypothesis $H_0 : \tau^{(1 \times 2 \times 3)} = 0$ is approximated by a scaled chi-square distribution $\hat{\gamma}_I\chi_{\hat{\nu}_I}^2$. To do this, let $\Sigma = \sigma^2\mathbf{I} + \tau^{(1)}\mathbf{K}^{(1)} + \tau^{(2)}\mathbf{K}^{(2)} + \tau^{(3)}\mathbf{K}^{(3)} + \tau^{1 \times 2}\mathbf{K}^{(1 \times 2)} + \tau^{(1 \times 3)}\mathbf{K}^{(1 \times 3)} + \tau^{(2 \times 3)}\mathbf{K}^{(2 \times 3)}$, and $\tau^{(1)}, \tau^{(2)}, \tau^{(3)}, \tau^{(1 \times 2)}, \tau^{(1 \times 3)}, \tau^{(2 \times 3)}$, and σ^2 are model parameters under the null model $\mathbf{y} = \mathbf{X}\boldsymbol{\beta} + \mathbf{h}_{\mathbf{M}^{(1)}} + \mathbf{h}_{\mathbf{M}^{(2)}} + \mathbf{h}_{\mathbf{M}^{(3)}} + \mathbf{h}_{\mathbf{M}^{(1) \times \mathbf{M}^{(2)}}} + \mathbf{h}_{\mathbf{M}^{(1) \times \mathbf{M}^{(3)}}} + \boldsymbol{\epsilon}$. The score function Eq. (A.1) under the null hypothesis becomes

$$\begin{aligned} \left. \frac{\partial \ell_R}{\partial \tau^{(1 \times 2 \times 3)}} \right|_{\tau^{(1 \times 2 \times 3)}=0} &= -\frac{1}{2\sigma^2} [\text{tr}(\mathbf{W}_{01}\mathbf{K}^{(1 \times 2 \times 3)}) - (\mathbf{y} - \mathbf{X}\hat{\boldsymbol{\beta}})^T \Sigma^{-1} \mathbf{K}^{(1 \times 2 \times 3)} \Sigma^{-1} (\mathbf{y} - \mathbf{X}\hat{\boldsymbol{\beta}})] \\ &= -\frac{1}{2} [\text{tr}(\mathbf{W}_{01}\mathbf{K}^{(1 \times 2 \times 3)}) - \mathbf{y}^T \mathbf{W}_{01} \mathbf{K}^{(1 \times 2 \times 3)} \mathbf{W}_{01} \mathbf{y}] \end{aligned} \quad (\text{B.2})$$

where $\mathbf{W}_{01} = \Sigma^{-1} - \Sigma^{-1} \mathbf{X}(\mathbf{X}^T \Sigma^{-1} \mathbf{X})^{-1} \mathbf{X}^T \Sigma^{-1}$ is the projection matrix under the null hypothesis. The test statistic for the higher order interaction effect is as follows:

$$S_I(\boldsymbol{\tau}_I) = \frac{1}{2\sigma_0^2} \mathbf{y}^T \mathbf{W}_{01} \mathbf{K}^{(1 \times 2 \times 3)} \mathbf{W}_{01} \mathbf{y},$$

where $\boldsymbol{\tau}_I = (\tau^{(1)}, \tau^{(2)}, \tau^{(3)}, \tau^{(1 \times 2)})$. Similarly for overall effect test, we can use the Satterthwaite method to approximate the distribution of higher order intersection test statistic $S_I(\boldsymbol{\tau}_I)$ by a scaled chi-square distribution with a scaled γ_I and degree of freedom ν_I , i.e., $S_I(\boldsymbol{\tau}_I) \sim \gamma_I\chi_{\nu_I}^2$. The mean and variance of the test statistic $S_I(\boldsymbol{\tau}_I)$ are:

$$\text{E}[S_I(\boldsymbol{\tau}_I)] = \frac{1}{2} \text{tr}(\mathbf{W}_{01}\mathbf{K}^{(1 \times 2 \times 3)}) = \text{E}[\gamma_I\chi_{\nu_I}^2] = \gamma_I\nu_I, \text{ and}$$

$$\text{Var}[S_I(\boldsymbol{\tau}_I)] = \frac{1}{2} \text{tr}(\mathbf{W}_0\mathbf{K}^{(1 \times 2 \times 3)}\mathbf{W}_0\mathbf{K}^{(1 \times 2 \times 3)}) = \text{Var}[\gamma_I\chi_{\nu_I}^2] = 2\gamma_I^2\nu_I$$

where $\mathbf{K} = \mathbf{K}^{(1)} + \mathbf{K}^{(2)} + \mathbf{K}^{(3)} + \mathbf{K}^{(1 \times 2)} + \mathbf{K}^{(1 \times 3)} + \mathbf{K}^{(2 \times 3)} + \mathbf{K}^{(1 \times 2 \times 3)}$, $\gamma_I = \frac{\text{Var}[S_I(\boldsymbol{\tau}_I)]}{2\text{E}[S_I(\boldsymbol{\tau}_I)]}$ and $\nu_I = \frac{2\text{E}[S_I(\boldsymbol{\tau}_I)]}{\text{Var}[S_I(\boldsymbol{\tau}_I)]}$, respectively. In practice, the unknown model parameters $\tau^{(1)}, \tau^{(2)}, \tau^{(3)}, \tau^{(1 \times 2)}, \tau^{(1 \times 3)}, \tau^{(2 \times 3)}$, and σ^2 are estimated by their respective ReML estimates $\hat{\tau}^{(1)}, \hat{\tau}^{(2)}, \hat{\tau}^{(3)}, \hat{\tau}^{(1 \times 2)}, \hat{\tau}^{(1 \times 3)}, \hat{\tau}^{(2 \times 3)}$, and $\hat{\sigma}^2$ under the null hypothesis. The scaled parameter and degree of freedom are estimated by the MOM. Specif-

ically, $\hat{\gamma}_I = \frac{\text{Var}[\widehat{S}_I(\tau_I)]}{2E[\widehat{S}_I(\tau_I)]}$, and $\hat{\nu}_I = \frac{2E[\widehat{S}_I(\tau_I)]}{\text{Var}[\widehat{S}_I(\tau_I)]}$, where $E[\widehat{S}_I(\tau_I)] = \frac{1}{2}\text{tr}(\mathbf{W}_0\mathbf{K}^{(1 \times 2 \times 3)})$ and $\text{Var}[\widehat{S}_I(\tau_I)] = \frac{1}{2}\text{tr}(\mathbf{W}_0\mathbf{K}^{(1 \times 2 \times 3)}\mathbf{W}_0\mathbf{K}^{(1 \times 2 \times 3)}) - \frac{\Delta\xi^{-1}\Delta}{2}$, in which

$$\Delta = [\text{tr}(\mathbf{B}^{(1 \times 2 \times 3)}\mathbf{W}_0) \quad \text{tr}(\mathbf{B}^{(1 \times 2 \times 3)}\mathbf{B}^{(1)}) \quad \text{tr}(\mathbf{B}^{(1 \times 2 \times 3)}\mathbf{B}^{(2)}) \quad \text{tr}(\mathbf{B}^{(1 \times 2 \times 3)}\mathbf{B}^{(3)}) \quad \text{tr}(\mathbf{B}^{(1 \times 2 \times 3)}\mathbf{B}^{(1 \times 2)}) \quad \text{tr}(\mathbf{B}^{(1 \times 2 \times 3)}\mathbf{B}^{(1 \times 3)}) \quad \text{tr}(\mathbf{B}^{(1 \times 2 \times 3)}\mathbf{B}^{(2 \times 3)})]$$

$$\xi = \begin{bmatrix} \text{tr}(\mathbf{W}_0^2) & \text{tr}(\mathbf{W}_0\mathbf{B}^{(1)}) & \text{tr}(\mathbf{W}_0\mathbf{B}^{(2)}) & \text{tr}(\mathbf{W}_0\mathbf{B}^{(3)}) & \text{tr}(\mathbf{W}_0\mathbf{B}^{(1 \times 2)}) & \text{tr}(\mathbf{W}_0\mathbf{B}^{(1 \times 3)}) & \text{tr}(\mathbf{W}_0\mathbf{B}^{(2 \times 3)}) \\ \text{tr}(\mathbf{W}_0\mathbf{B}^{(1)}) & \text{tr}(\mathbf{B}^{(1)}\mathbf{B}^{(1)}) & \text{tr}(\mathbf{B}^{(1)}\mathbf{B}^{(2)}) & \text{tr}(\mathbf{B}^{(1)}\mathbf{B}^{(3)}) & \text{tr}(\mathbf{B}^{(1)}\mathbf{B}^{(1 \times 2)}) & \text{tr}(\mathbf{B}^{(1)}\mathbf{B}^{(1 \times 3)}) & \text{tr}(\mathbf{B}^{(1)}\mathbf{B}^{(2 \times 3)}) \\ \text{tr}(\mathbf{W}_0\mathbf{B}^{(2)}) & \text{tr}(\mathbf{B}^{(2)}\mathbf{B}^{(1)}) & \text{tr}(\mathbf{B}^{(2)}\mathbf{B}^{(2)}) & \text{tr}(\mathbf{B}^{(2)}\mathbf{B}^{(3)}) & \text{tr}(\mathbf{B}^{(2)}\mathbf{B}^{(1 \times 2)}) & \text{tr}(\mathbf{B}^{(2)}\mathbf{B}^{(1 \times 3)}) & \text{tr}(\mathbf{B}^{(2)}\mathbf{B}^{(2 \times 3)}) \\ \text{tr}(\mathbf{W}_0\mathbf{B}^{(3)}) & \text{tr}(\mathbf{B}^{(3)}\mathbf{B}^{(1)}) & \text{tr}(\mathbf{B}^{(3)}\mathbf{B}^{(2)}) & \text{tr}(\mathbf{B}^{(3)}\mathbf{B}^{(3)}) & \text{tr}(\mathbf{B}^{(3)}\mathbf{B}^{(1 \times 2)}) & \text{tr}(\mathbf{B}^{(3)}\mathbf{B}^{(1 \times 3)}) & \text{tr}(\mathbf{B}^{(3)}\mathbf{B}^{(2 \times 3)}) \\ \text{tr}(\mathbf{W}_0\mathbf{B}^{(1 \times 2)}) & \text{tr}(\mathbf{B}^{(1 \times 2)}\mathbf{B}^{(1)}) & \text{tr}(\mathbf{B}^{(1 \times 2)}\mathbf{B}^{(2)}) & \text{tr}(\mathbf{B}^{(1 \times 2)}\mathbf{B}^{(3)}) & \text{tr}(\mathbf{B}^{(1 \times 2)}\mathbf{B}^{(1 \times 2)}) & \text{tr}(\mathbf{B}^{(1 \times 2)}\mathbf{B}^{(1 \times 3)}) & \text{tr}(\mathbf{B}^{(1 \times 2)}\mathbf{B}^{(2 \times 3)}) \\ \text{tr}(\mathbf{W}_0\mathbf{B}^{(1 \times 3)}) & \text{tr}(\mathbf{B}^{(1 \times 3)}\mathbf{B}^{(1)}) & \text{tr}(\mathbf{B}^{(1 \times 3)}\mathbf{B}^{(2)}) & \text{tr}(\mathbf{B}^{(1 \times 3)}\mathbf{B}^{(3)}) & \text{tr}(\mathbf{B}^{(1 \times 3)}\mathbf{B}^{(1 \times 2)}) & \text{tr}(\mathbf{B}^{(1 \times 3)}\mathbf{B}^{(1 \times 3)}) & \text{tr}(\mathbf{B}^{(1 \times 3)}\mathbf{B}^{(2 \times 3)}) \\ \text{tr}(\mathbf{W}_0\mathbf{B}^{(2 \times 3)}) & \text{tr}(\mathbf{B}^{(2 \times 3)}\mathbf{B}^{(1)}) & \text{tr}(\mathbf{B}^{(2 \times 3)}\mathbf{B}^{(2)}) & \text{tr}(\mathbf{B}^{(2 \times 3)}\mathbf{B}^{(3)}) & \text{tr}(\mathbf{B}^{(2 \times 3)}\mathbf{B}^{(1 \times 2)}) & \text{tr}(\mathbf{B}^{(2 \times 3)}\mathbf{B}^{(1 \times 3)}) & \text{tr}(\mathbf{B}^{(2 \times 3)}\mathbf{B}^{(2 \times 3)}) \end{bmatrix},$$

where $\mathbf{B}^{(1)} = \mathbf{W}_0\mathbf{K}^{(1)}$, $\mathbf{B}^{(2)} = \mathbf{W}_0\mathbf{K}^{(2)}$, $\mathbf{B}^{(3)} = \mathbf{W}_0\mathbf{K}^{(3)}$, $\mathbf{B}^{(1 \times 2)} = \mathbf{W}_0\mathbf{K}^{(1 \times 2)}$, $\mathbf{B}^{(1 \times 3)} = \mathbf{W}_0\mathbf{K}^{(1 \times 3)}$, $\mathbf{B}^{(2 \times 3)} = \mathbf{W}_0\mathbf{K}^{(2 \times 3)}$, $\mathbf{B}^{(1 \times 2 \times 3)} = \mathbf{W}_0\mathbf{K}^{(1 \times 2 \times 3)}$. The p -value of an observed higher order interaction effect test score statistic $S_I(\tau_I)$ is obtained using the scaled chi-square distribution $\hat{\gamma}_I\chi_{\hat{\nu}_I}^2$.

C Supplementary figures and tables

Table 5: The selected significant genes-derived SNP, ROIs and gene-derived DNA methylation using the proposed method (KMDHOI). The p -values threshold was fixed to 0.01.

Genetics	Imaging	Epigenetics	σ^2	$\tau^{(1)}$	$\tau^{(2)}$	$\tau^{(3)}$	KMDHOI				OVA	HOI
							$\tau^{1 \times 2}$	$\tau^{1 \times 3}$	$\tau^{2 \times 3}$	$\tau^{1 \times 2 \times 3}$		
BDNF	AMYG.L	DUSP1	0.5658	0.0559	0.0887	0.0041	0.0494	2.1147	0.0000	0.0100	0.0345	0.0069
BDNF	CRBL10.L	FBXO28	0.5589	0.0334	0.1414	0.0157	1.2657	0.0000	0.2034	0.0100	0.0102	0.0058
BDNF	CRBL3.R	DUSP1	0.4255	0.2077	0.0000	0.0556	0.7339	2.1418	1.0345	0.0100	0.0414	0.0072
BDNF	ORBsup.L	FBXO28	0.5515	0.0033	0.4506	0.0535	0.8534	0.6955	0.0000	0.0100	0.0078	0.0013
BDNF	LING.R	CRABP1	0.5510	0.5258	0.2416	0.0640	0.9032	0.7442	0.0000	0.0100	0.0114	0.0074
BDNF	IPL.R	FBXO28	0.4471	0.0388	0.1458	0.0644	1.2503	2.3689	0.0000	1.9045	0.0367	0.0024
CHGA	AMYG.L	HOXA9	0.4326	0.0027	0.3130	0.3598	1.5185	0.0000	1.1948	0.7093	0.0474	0.0075
CHGB	CRBL3.L	DUSP1	0.6779	0.0321	0.1444	0.1232	0.2505	0.5545	0.0000	0.0100	0.0454	0.0025
CHGB	DCG.L	DUSP1	0.5253	0.0247	0.0213	0.0570	1.2794	1.0467	0.0000	0.0100	0.0408	0.0035
CHGB	STG.L	DUSP1	0.5415	0.1053	0.0360	0.0017	1.1720	1.2059	0.0000	0.0100	0.0293	0.0035
CLINT1	IPL.R	GPSN2	0.4074	0.6728	0.0404	0.0514	1.2476	1.6953	0.0000	0.0100	0.0228	0.0042
COMTD1	ROL.R	FBXO28	0.5717	0.0740	0.0095	0.0479	2.5561	0.3378	0.0000	2.3490	0.0370	0.0083
DAOA	ORBsup.L	DUSP1	0.3721	0.1079	0.0731	0.0097	0.5586	3.5344	0.0000	0.0100	0.0490	0.0012
DISC1	IPL.R	PLAGL1	0.3370	0.0161	0.0547	0.1417	1.5286	3.2871	0.0000	1.4004	0.0439	0.0029
DRD2	ORBsup.R	DUSP1	0.3772	0.0000	0.3189	0.0073	1.1268	2.0353	0.9757	0.0100	0.0445	0.0062
DTNBP1	IPL.R	SRF	0.3940	0.1987	0.0637	0.2312	1.4537	1.8458	0.0000	0.0100	0.0267	0.0037
ERBB4	CRBLCrus2.R	DUSP1	0.2576	0.0000	0.0413	0.0401	1.2244	3.1904	1.0830	0.0100	0.0459	0.0088
ERBB4	IPL.R	FEN1	0.4484	0.0000	0.0762	0.0357	0.8799	2.9942	0.1061	0.0100	0.0294	0.0074
ERBB4	IPL.R	HOXB4	0.3308	0.6704	0.0669	0.0222	2.3489	1.9820	0.0000	0.0100	0.0396	0.0082
GABBR1	LING.R	CRABP1	0.5610	0.0068	0.4045	0.0563	1.8524	0.0000	0.7076	0.0100	0.0166	0.0072
GABRB2	SMA.R	EDNRB	0.5276	0.0139	0.1276	0.0364	1.3359	2.4832	0.0000	2.0971	0.0283	0.0061
GRIN2B	IPL.R	HOXB4	0.3523	0.2359	0.0352	0.0297	2.1599	2.1357	0.0000	0.0100	0.0421	0.0012
GRM3	SMA.R	EYA4	0.6435	0.0088	0.3928	0.0384	0.5390	1.5425	0.0000	0.4976	0.0237	0.0024
HTR2A	ITG.L	FBXO28	0.4496	0.3074	0.0087	0.0970	0.1874	2.0080	0.0000	0.0100	0.0211	0.0016
IL10RA	LING.L	CRABP1	0.5128	0.1846	0.1055	0.0436	1.3817	0.0000	0.1076	0.0100	0.0373	0.0035
IL10RA	TPOsup.R	CRABP1	0.5644	0.2024	0.0000	0.0364	1.3936	1.1762	0.0700	0.0100	0.0425	0.0098
IL1B	AMYG.L	FBXO28	0.5708	0.0130	0.4484	0.0755	1.8572	0.0000	0.3580	1.0757	0.0445	0.0040
IL1B	CAU.R	FBXO28	0.6755	0.0038	0.0229	0.1225	1.1013	0.0000	0.1307	1.3606	0.0383	0.0002
IL1B	PoCG.R	FBXO28	0.5837	0.0189	0.1827	0.1247	1.8403	0.0000	0.3469	1.0603	0.0202	0.0007
MAGI1	CRBL6.L	CRABP1	0.3178	0.5873	0.0201	0.0249	1.7962	1.7014	0.0000	0.0100	0.0346	0.0045
MAGI2	CRBLCrus1.L	FBXO28	0.1833	0.3246	0.0000	0.2693	1.1963	2.2426	1.3683	0.0100	0.0288	0.0000
MAGI2	DCG.R	FBXO28	0.3211	0.0000	0.1485	0.0513	2.0150	2.5252	0.3083	0.0100	0.0298	0.0057

Table 6: Table 5 continued:

Genetics	Imaging	Epigenetics	σ^2	$\tau^{(1)}$	$\tau^{(2)}$	$\tau^{(3)}$	KMDHOI				OVA	HOI
							$\tau^{1 \times 2}$	$\tau^{1 \times 3}$	$\tau^{2 \times 3}$	$\tau^{1 \times 2 \times 3}$		
MAGI2	LING.L	CRABP1	0.1813	0.4366	0.0000	0.0885	1.5370	2.6299	1.0271	0.0100	0.0470	0.0000
MAGI2	IPL.R	SRF	0.2510	0.2349	0.0325	0.2015	1.4611	3.1453	0.0000	0.0100	0.0198	0.0087
MAGI2	IPL.L	FBXO28	0.1833	0.3778	0.0000	0.3044	0.9808	2.3888	1.2203	0.0100	0.0457	0.0000
MICB	Vermis3	FBXO28	0.6579	0.0806	0.0199	0.0444	0.0000	0.2964	0.4610	0.0100	0.0458	0.0060
NOS1AP	IPL.R	DUSP1	0.2939	0.0000	0.2870	0.3240	0.8961	1.8125	1.2330	0.0100	0.0185	0.0012
NOTCH4	Vermis3	FBXO28	0.7878	0.0000	0.0183	0.0896	0.3783	0.2783	0.0057	1.1039	0.0256	0.0054
NR4A2	PAL.R	CRABP1	0.4953	0.1173	0.0000	0.0237	1.4544	0.3867	0.7814	0.0100	0.0491	0.0078
NRG1	IPL.R	PLAGL1	0.3682	0.0024	0.2162	0.1270	1.1227	2.7930	0.0000	0.2056	0.0284	0.0000
NUMBL	ORBsup.R	CDKN1A	0.5418	0.0585	0.4680	0.0865	0.6606	0.4765	0.0000	0.0100	0.0479	0.0065
PDLIM5	ORBsup.R	CCND2	0.4108	0.0109	0.4396	0.2792	0.0000	2.5753	0.2739	2.2025	0.0437	0.0016
PDLIM5	IPL.R	DUSP1	0.3648	0.0000	0.0804	0.2182	1.5177	1.9409	1.0276	0.0100	0.0183	0.0005
PDLIM5	IPL.R	PLAGL1	0.3134	0.0000	0.2173	0.2447	1.5550	1.8347	1.5020	0.0100	0.0460	0.0027
PDLIM5	PoCG.R	DUSP1	0.3598	0.0000	0.2256	0.0139	0.9189	1.7853	1.2796	0.0100	0.0498	0.0004
PLXNA2	SMA.R	RB1	0.2386	0.2186	0.2257	0.0341	0.8229	3.2966	0.0000	0.0100	0.0432	0.0017
PPP3CC	IPL.R	FBXO28	0.7594	0.0000	0.1627	0.0338	0.8919	0.5701	0.6865	0.0100	0.0199	0.0012
SLC18A1	ORBsup.R	FHIT	0.4096	0.0065	0.5356	0.2276	1.3456	0.0000	1.0003	0.1323	0.0495	0.0001
SLC18A1	ORBsup.R	PLAGL1	0.2869	0.0000	0.3909	0.1933	1.0186	1.3148	1.3676	0.0100	0.0373	0.0003
SLC18A1	Vermis45	TFPI2	0.5571	0.0447	0.0815	0.0020	0.0000	1.0458	0.5579	0.0100	0.0354	0.0007
SNAP29	ORBsup.R	DUSP1	0.5384	0.0333	0.3235	0.0685	0.2128	1.3135	0.0000	0.0100	0.0417	0.0039
TDRD3	CRBL10.R	EDNRB	0.5890	0.3319	0.0000	0.0310	0.9546	0.5359	0.8984	0.0100	0.0236	0.0025
TDRD3	CRBL3.L	EYA4	0.5162	0.1651	0.1782	0.0612	0.4628	0.4991	0.0000	0.0100	0.0180	0.0019
TDRD3	CRBL45.L	CCND2	0.5346	0.0523	0.2672	0.1649	0.3055	1.1277	0.0000	0.0100	0.0124	0.0019
TDRD3	CRBL8.L	FBXO28	0.5856	0.2284	0.0022	0.0702	1.1722	0.7667	0.0000	0.0100	0.0052	0.0000
TDRD3	CRBL8.L	ZNF512	0.5627	0.2690	0.0000	0.0375	0.7126	0.7087	1.3420	0.0101	0.0196	0.0021
TDRD3	CRBLCrus1.L	WDR37	0.5287	0.1848	0.0563	0.0201	1.4667	0.6084	0.0000	0.0100	0.0423	0.0076
TDRD3	CRBLCrus2.L	DUSP1	0.4862	0.2265	0.3120	0.0235	0.0000	1.2779	0.6463	0.0100	0.0185	0.0047
TDRD3	DCG.R	EYA4	0.5874	0.1843	0.3626	0.0010	0.5656	0.1007	0.0000	0.0100	0.0135	0.0028
TDRD3	PCG.R	DUSP1	0.8170	0.1434	0.0746	0.0690	0.0000	0.3873	0.0623	0.0100	0.0082	0.0079
TDRD3	PCG.R	PTGS2	0.8223	0.1481	0.1251	0.0182	0.1414	0.5447	0.0000	0.0100	0.0256	0.0040
TDRD3	ORBsup.L	FBXO28	0.5762	0.1398	0.3331	0.0679	0.8560	0.4102	0.0000	0.0100	0.0014	0.0050
TDRD3	ORBmid.R	HOXA9	0.7235	0.3465	0.0000	0.2839	0.8353	0.5320	0.1433	0.0100	0.0067	0.0073
TDRD3	LING.L	ZNF512	0.6416	0.0308	0.0000	0.1771	1.4260	0.3854	0.0717	0.0100	0.0312	0.0098
TDRD3	CAU.R	CCND2	0.6381	0.1076	0.0170	0.0635	0.7395	1.2557	0.0000	0.0100	0.0096	0.0021
TDRD3	IPL.L	ZNF512	0.6093	0.2597	0.0520	0.0380	1.0761	0.9126	0.0000	0.0100	0.0180	0.0018
TDRD3	TPOsup.L	PLAGL1	0.6437	0.1242	0.0000	0.1318	0.0209	0.8248	0.3640	1.6934	0.0374	0.0024
TDRD3	MTG.R	CCND2	0.2905	0.3650	0.0000	0.5177	0.8603	1.2746	1.6902	0.0100	0.0334	0.0040
TDRD3	ITG.R	CRABP1	0.5291	0.2318	0.0000	0.0223	0.7052	0.6038	0.6240	0.0100	0.0033	0.0004
TDRD3	ITG.R	EDNRB	0.4778	0.3792	0.0000	0.0265	1.0527	1.1174	0.9571	0.0100	0.0243	0.0085
TDRD3	Vermis10	FEN1	0.3894	0.5985	0.0000	0.0103	0.7989	1.4191	0.9878	0.0100	0.0377	0.0037
TDRD3	Vermis45	PTGS2	0.7504	0.1816	0.0718	0.0085	0.0000	0.4176	0.3236	0.0100	0.0121	0.0073

Table 7: A part of 31 genes-derived SNP annotation using DAVID software.

Annotation	Database	Term	No. genes	P-Value	Benjamini
Literature	Pubmed-ID	19367581	12	$1.6E - 22$	$5.8E - 19$
		18198266	7	$3.0E - 15$	$5.5E - 12$
		19328558	8	$1.1E - 13$	$1.4E - 10$
		19086053	11	$5.3E - 13$	$4.9E - 102$
		12477932	31	$4.4E - 6$	$1.8E - 3$
		15489334	21	$5.5E - 5$	$.3E - 2$
Disease	GADB-disease-class	Schizophrenia	26	$1.1E - 26$	$4.4E - 24$
		Cognitive function	6	$4.4E - 6$	$8.9E - 4$
		Bipolar disorder	6	$1.5E - 3$	$9.8E - 2$
Gene-Ontology	GOTERM-BP-1	multicellular organismal process	17	$1.3E - 4$	$2.4E - 3$
		Developmental process	13	$1.7E - 3$	$2.4E - 3$
Pathways	KEGG	Neuroactive ligand – receptor interaction	6	$2.0E - 3$	$6.6E - 2$
	PANTHER	P05912	4	$7.8E - 3$	$2.6E - 1$
		P00001	3	$9.0E - 3$	$1.6E - 1$
Protein Interactions	UCSC	HFH3	22	$2.5E - 5$	$4.4E - 3$
		BRN2	24	$4.8E - 5$	$4.2E - 3$
		CDP	24	$1.6E - 3$	$9.0E - 3$
		GATA	20	$1.8E - 3$	$9.2E - 3$